Cement and Concrete Research 155 (2022) 106782

Contents lists available at ScienceDirect

Cement and Concrete Research

journal homepage: www.elsevier.com/locate/cemconres

A chemical process engineering look at digital concrete processes: critical step design, inline mixing, and scaleup

Timothy Wangler [a,*], Rafael Pileggi [b], Seyma Gürel [a], Robert J. Flatt [a]

[a] Institute for Building Materials, ETH Zurich, Zurich, Switzerland
[b] Department of Construction Engineering, University of São Paolo, São Paolo, Brazil

ARTICLE INFO

Keywords:
Digital fabrication
Concrete
3D printing
Extrusion
Mixing

ABSTRACT

Digital concrete processes are a series of unit operations, similar to a chemical engineering process, each subject to their own rheological and other performance requirements, such as homogeneity, etc. In this article we examine the concrete extrusion 3D-printing process from this standpoint, first decomposing it into individual unit operations. We examine the role that residence time distributions play in the overall process, and then analyze how large scale printing to structural heights could be performed continuously. We then focus on the critical step of secondary (inline) mixing just before extrusion from the standpoint of mixing processes in the chemical processing industries. This unit operation is then analyzed in the context of scaleup to larger print areas and larger flowrates, finding that increase in viscosity plays a major role in power requirements and printhead mass. Further research questions are then raised based on these analyses.

1. Introduction

Digital fabrication with concrete has exploded onto the scene as a hot research topic in the civil engineering materials and structures community, especially within the past decade [1–5]. The primary motivating factors driving this technology's implementation in the construction sector have to do with both sustainability and cost considerations: implementation of more customized, materially efficient designs now has an easier path, and even the construction of standard designs, impacted in many economies by a lack of skilled labor, has now potentially an automated solution [3,4]. These factors combined with the rapid advancement of robotic technology have made large scale demonstrations now a more frequent occurrence [6,7]. However, numerous challenges remain in making this a viable technological solution in the construction sector, with the primary challenges being the implementation of reinforcement [8,9] and the development of reliable and robust materials and processing systems capable of operating at the required scales [3].

The nascent concrete 3D printing industry has apparently established a benchmark of 3D printing an entire building within 24 h [10–12]. This benchmark, and claims of achieving it, has been the subject of some controversy. Aside from the fact that a building is much more than its vertical walls and columns, most claims have turned out to be purely based on printing times, not accounting for pauses [13,14], and the goal of achieving the high vertical build rates to reach this benchmark at these scales has not yet been met once, to the authors' knowledge, much less in a reliable and consistent way. Thus, consistently achieving adequate vertical building rates at larger area scales remains an issue to be addressed.

Additionally, on the material side, it has been noted that cementitious mixes for digital fabrication have much higher cement contents than normal concretes [15–17], which has to do with a number of factors:

1) For processability, the mixes require high paste contents, of which the ordinary Portland cement (OPC) is a major component,
2) Again for processability and due to equipment limitations (in pumping or mixing), the maximum aggregate size is limited (often to <4 mm)
3) Set control of these mixes (if implemented) often scales with OPC content, and the needed early strength is easier to reach with high OPC mixes when using commercially available set accelerators.

The major industrial use cases of this technology to date have been to use the printing technology as a replacement for formwork labor (e.g. printing lost formworks) or as a replacement for masonry labor (e.g.

* Corresponding author.
E-mail address: wangler@ifb.baug.ethz.ch (T. Wangler).

https://doi.org/10.1016/j.cemconres.2022.106782
Received 11 December 2021; Received in revised form 19 February 2022; Accepted 15 March 2022
Available online 23 March 2022

printing unreinforced masonry) [7]. Thus, this has meant that on a material, per-unit basis, printed structures have considerably worse carbon footprints than the structures they are meant to replace [18]. It is imperative then for the research community to solve or mitigate these issues through 1) decreasing paste content through better mix design, including increased maximum aggregate size, and 2) developing set accelerated mixes with lower OPC contents on a per-unit basis (i.e. highly blended cements).

Addressing the challenges of set acceleration of low OPC systems and increasing aggregate size has already started in the literature, notably with Boscaro et al. [16] and da Silva et al. [19] demonstrating set acceleration of highly blended cements, and the full-scale printing of structures with coarse aggregates by the US Army Corps of Engineers [20] and also commercially by companies such as COBOD [21]. Da Silva et al. [19] as well as Burger et al. [22] have also shown that set acceleration of digitally processed coarse aggregate mixes is indeed possible. However, the combination of coarse aggregates and reliable set acceleration remains elusive at the larger scales, in particular for 3D extrusion printing.

To date, an attempt at critically and systematically examining digital fabrication with concrete through the lens of process engineering has not been performed, in spite of a wealth of available literature from the process engineering community related to important unit operations such as mixing [23–26]. It is the aim of this paper to fill this gap, especially for the dominant process of 3D extrusion based printing of cementitious materials [2,27], doing this through the process engineering eye and addressing the particularly important points relating to scaleup: increased aggregate size, and higher processing rates across larger processing areas. We first briefly review and examine the major steps of all digital concrete processes, before honing in on the highly critical secondary (inline) mixing step. We then perform an analysis of this step in the context of scaleup, and give recommendations for future research.

2. Digital concrete processing

All digital concrete processes consist of a series of steps, with the goal of the production of an end product: self-supported 3D printed material. The major steps are identified in Fig. 1 and defined below. The underlying physics of many of these steps has also previously been analyzed in [27]. Certain steps in this processing chain impose limitations on the other steps, and each step can be conducted as a batch or a continuous flow process, which is highlighted in Fig. 1.

2.1. Processing steps

2.1.1. Mix proportioning

Mix proportioning (step 1) is the process of weighing of defined quantities of dry materials, water, chemical admixtures and other mix components. This is almost always done via batch processing. Sometimes, this is done on an ad hoc basis, but increasingly the dominant method is through pre-dosing into drymix batches to which water (and sometimes chemical admixtures) is added during primary mixing. It is also possible to perform this step on a continuous basis through the use of volumetric mixers [29].

2.1.2. Primary (1st) mixing

Primary mixing is the step (2) in which water is initially added to the dry materials. Mechanical energy is used to disperse the dry materials homogeneously, and to initiate contact between water and the dry materials, ideally distributing water to homogeneously cover all solid particles, as well as effectively dispersing the chemical admixtures throughout. While it has not necessarily been well studied compared to other aspects of concrete processing, it is the only mixing step for which there has been interest for cementitious materials, especially in the context of high performance concretes and impact on hydration [30–35]. This mixing operation is commonly performed in a batch mixer, but many 3D printing systems are carrying it out continuously using commercially available continuous mixers [36]. Normal mixing times are on the order of a few seconds to minutes [35,37].

2.1.3. Storage

Especially in systems using batch mixers, there is a step in which the material is stored before being fed into a pumping system. This storage operation (step 3) is usually performed via batches, however, there are hopper systems feeding the material into pump screws that also function as storage. This unit operation can sometimes precede other parts of the process as well; for example, in the COBOD printing system, there is a hopper that feeds the rotor/stator of the printhead [38]. This is also noted in Fig. 1a (step 5 for 1 K systems).

2.1.4. Transport/material delivery

Transport (step 4) consists of the delivery of the material to the printhead. This step is almost exclusively carried out by pumping. Most published systems utilize progressive cavity pumps (rotor/stator) to carry out this operation, although positive displacement piston pumps can be used as well [27,39,40]. Pumping of concrete and other cementitious materials has been well analyzed [41–43], although there are some specificities in pumping of 3D printable materials discussed recently by Mechtcherine et al. [27], such as the fact that most of these materials generally have a high yield stress and thixotropy, unless they are activated at the printhead, in which case they generally have lower yield stresses and are more fluid.

2.1.5. Secondary (2nd) mixing

The secondary mixing step involves the injection of an additive at the printhead for stiffening control to enhance buildability, and has been discussed in the following [44,45]. Other additives can also be injected as well, such as pigments. Generally, this step has been performed by an active mixer [28,46–48], although static mixers have recently been employed [45,49]. This step is not exclusive to 3D printing, as it has been standard in application of shotcrete in the wet-mix process, where mixing between accelerator and the sprayed concrete occur upon injection before spraying from the nozzle [45]. In Fig. 1, the distinction between 1 component (1K) and 2 component (2K) systems is made, in which this step (5, for 2K systems) is the defining difference, described in more detail later in Section 2.3.

2.1.6. Application

The application step (6) in concrete 3D extrusion printing is the extrusion itself from the printhead. The material has specific requirements here, primarily linked to the expected shape of the filament after extrusion, and well-reviewed in [27,40,50]. The filament must of course be able to hold its own shape, but must also be not so stiff that it leads to cracking. Two boundaries on the filament shape are noted: 1) the “infinite brick”, characterized by a high yield stress and a limited shear zone across the filament, and 2) the highly fluid, fully sheared filament, with a low but rapidly evolving yield stress [50]. Very often, 1K processes have “infinite brick” filaments, while 2K processes have more fluid filaments to facilitate processing in the printhead [27]. In other digital concrete processes such as the Digital Casting processes, this step has somewhat different requirements, requiring an even lower yield stress initially in order to flow and fill the mold, before a rapid growth in yield stress is initiated [51].

2.1.7. Finishing

Certain technologies have a finishing step (7), in which the concrete, in its still workable state, is finished by some type of shaping mechanism. This can be incorporated directly with the extrusion step, as has been seen in the Contour Crafting process via robotically controlled trowels [52], or it can be performed some time afterward mechanically, as is done in the metal formwork supported shotcrete process in [53].

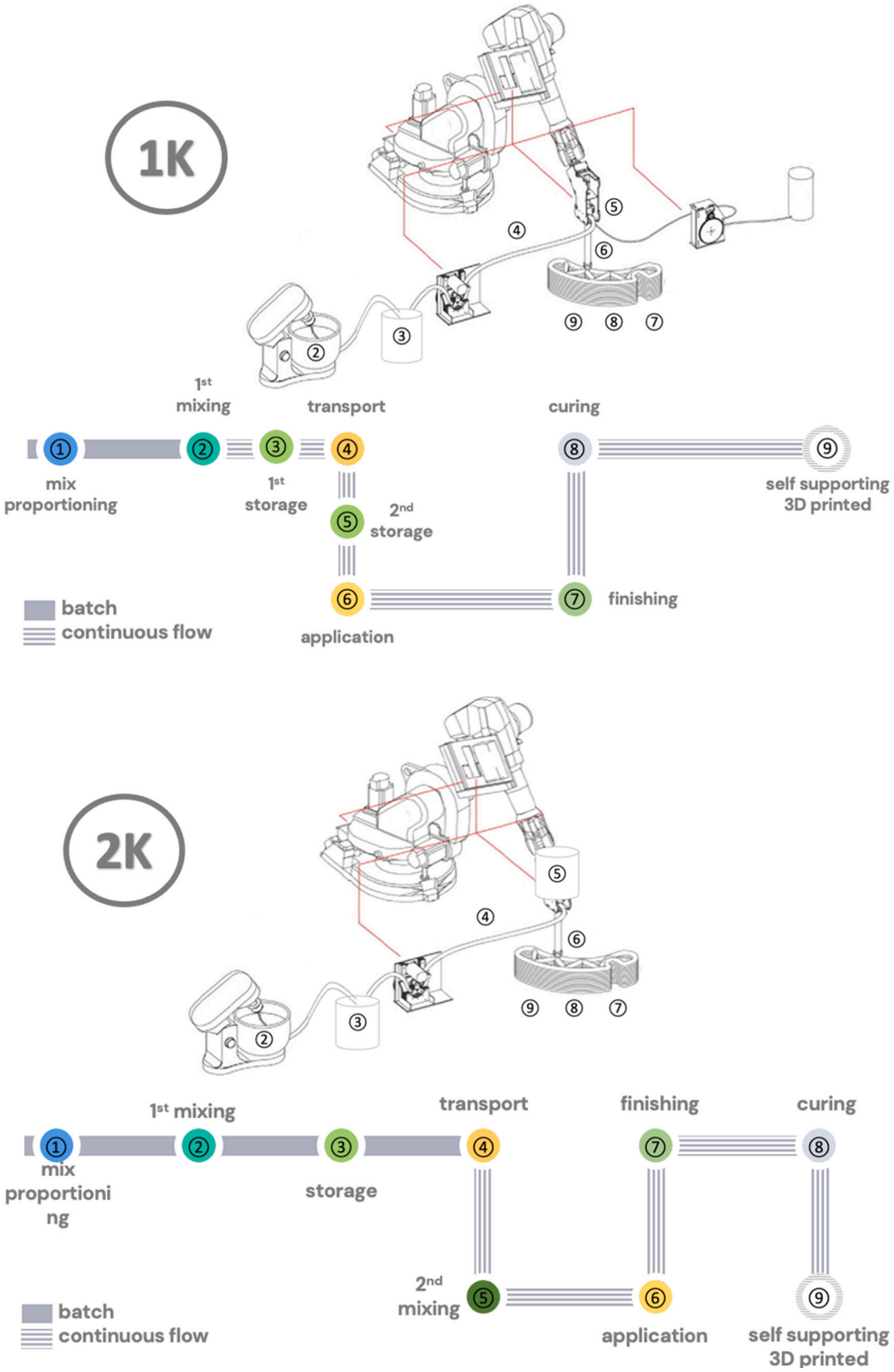

Fig. 1. Illustration of various processing steps in concrete extrusion 3D printing processes. 1 component systems (1K) do not include the secondary mixing step of an accelerator just before extrusion, as in the 2 component (2K) systems. Robotic figure adapted from [28].

2.1.8. Curing (strength buildup)

The curing step (8) can be defined in the context of 3D printing, for this analysis, as the step in which the concrete is building its strength to support further layers. This step is required for so-called "buildability" to be achieved, as a lack of evolution of strength will eventually result in the collapse of the printed structure. A material with adequate strength buildup will lead to the ultimate process goal, which is a self-supporting 3D printed material. It should be noted, however, that the curing step can also include crucial processes related to moisture management, potentially critical for avoiding "cold joints" [54,55].

2.2. Residence time distributions

Understanding residence times and residence time distributions (RTDs) is critical to any process engineering undertaking involving flow processes [26,56,57]. The introduction of this concept by Danckwerts [58] was seminal in the chemical process engineering industry, and applies as importantly to digital concrete processing. While much attention in digital concrete processing has focused on spatial homogeneity, the concept of RTD is focused on temporal homogeneity: the digital concrete processes are in the most basic sense the movement and processing of a reactive material, one that transitions in ease of processing with time, therefore the age and the age distribution of the processed material is highly critical. Recently, Wangler et al. introduced this concept to the digital concrete processes [59], and it is briefly summarized below.

In any processing step, the average residence time t_R is defined as the average amount of time the material or species spends within a specific volume or space. This is easily calculated based on the volumetric flowrate of the material, Q, and the volume, V, that the material has to flow through during that time:

$$t_R = \frac{V}{Q} \tag{1}$$

Every step of the entire processing chain in Fig. 1 up to the extrusion of the concrete has a residence time, and an associated RTD. An important concept to aid in understanding RTDs is the concept of a washout function, $W(t)$, which represents the response of the system to a negative step change of a component in the system (such as suddenly stopping the injection of a tracer) [60]. The washout function gives the proportion of the material still in the system at a given time. It is often given in terms of dimensionless time (t/t_R), in which the time is scaled by the average residence time.

There are different flow regimes which exhibit different behaviors, but the simplest one to understand is that of the batch reactor. For example, if primary mixing takes place in a batch mixer, the average residence time is simply the difference in time between input and discharge of the materials, and the washout function resembles a step function, as everything leaves the mixer at exactly the same time, as seen in Fig. 2.

In flow systems, the behavior becomes more complicated. There are in reality three main flow models which have been evaluated analytically: 1) plug flow, 2) laminar flow, and 3) continuously stirred tank reactors (CSTR). In plug flow systems, the assumption is made of perfect radial mixing and no axial movement of material besides that imparted by the bulk flow, thus the washout function is identical to that of the batch mixer: a step function at the average residence time. In laminar flow systems, the no-slip condition at the wall boundary combined with the gradient in shear leads to a parabolic velocity distribution, which means material close to the wall spends, on average, a longer time in the volume than material in the center, leading to a distribution of residence times centered around the average and a dispersed washout function. In continuously stirred systems, it is assumed that mixing is perfect and that uniform dispersion is achieved instantly so all concentrations are equal throughout the volume and the outlet. This leads to a washout function that is exponential and exhibits the broadest dispersion of these

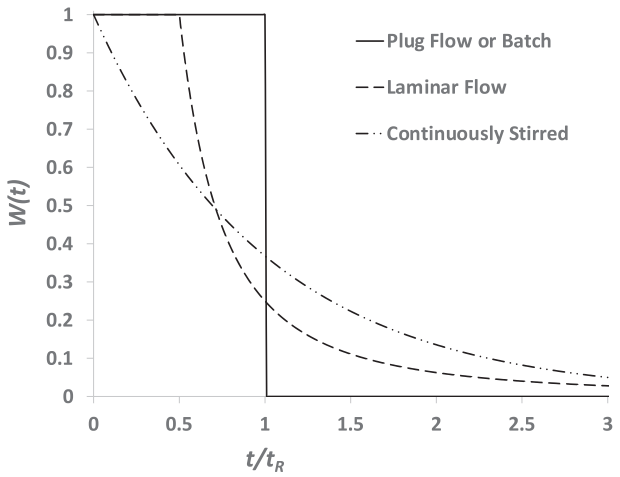

Fig. 2. Residence time distributions (given by washout function vs. time normalized by residence time) of various reactor models. Some models show immediate discharge of all materials after the average residence time, while some show a distribution of residence times.

different flow regimes. All RTD washout functions are depicted in Fig. 2.

One can clearly see how a distribution of residence times, and thus a distribution of material age, requires consideration in process design. Even if the process is designed for a particular residence time, a certain fraction of the material may have a residence time that exceeds a limit. For example, in a CSTR, 13.5% of the material spends double the average residence time, and 5% of the material triple the average residence time in the reactor before exiting. Another such example was described by Reiter et al. [61], in which long pumping lines of accelerated material with a laminar flow velocity distribution can clearly lead to process degradation. As De Schutter and Feys [41] have pointed out that pumped concrete has a Reynolds number in the laminar regime, and given a laminar flow distribution, 12.5% of the material spends double the average residence time in a pipe, and 3% of the material spends triple the average residence time. When the volumes and associated residence times are small relative to the total processing time, these RTDs are of less consequence, but upon scaleup, they start to require attention.

In reality, the RTD of a real system is usually not exactly depicted by any single one of these ideal models, but has an intermediate behavior, which helps to underscore the importance of understanding RTDs in time-dependent reactive systems such as those in digital concrete. Various models to describe this intermediate behavior have been developed, such as, for example, those based on axial dispersion in tubular flow [26,56]. In addition, RTDs and their determination are critical to understanding potential processing pathologies [60,62]. For example, dead zones and channeling are usually identified in RTD experiments, in which a tracer concentration is either injected or suddenly increased or decreased.

2.3. Process engineering classification: 1K and 2K systems

Buswell et al. [63] developed a framework in which processes were classified especially with respect to the current frameworks present in the greater additive manufacturing community. DFC processes generally fell into the framework based on their primary shaping process, along with other sub-processes that were essential to the production of the manufactured part. The focus of this paper will be on extrusion of concrete as a primary process only, with no focus on subprocesses other than secondary mixing as a means of hydration control. We classify these, in parlance borrowed from the coatings community [64], as 1 component (1K) systems or 2-component (2K) systems, with major steps of each seen in Fig. 1. 2K systems essentially have all the processing steps

up to extrusion, and 1K systems omit the step of secondary mixing. Table 1 summarizes some of the features of major systems seen so far.

Up to now, on-site printing by large scale systems, which can cover tens of square meters of area, are exclusively 1K systems. This includes the most advanced commercially available printers, for example from COBOD, Apis Cor, Contour Crafting and ICON. 2K systems, such as those from Sika and Baumit, are currently occupying much smaller footprints to produce what are essentially prefabricated components at very rapid vertical building rates. Additionally, until now, there appears to have been no consistent large scale, continuous prints. Nearly every large-scale print has required stops after reaching a certain build height, a couple of examples of which are depicted in Fig. 3, although the respective companies do not state the cause. Clearly, these stops are not ideal, as such stops can exacerbate the formation of "cold joints" that have been shown to be problematic in terms of strength and durability even after layer interval times of just 10 min, depending on the material [74,75]. These stops are required for one of 3 likely reasons: 1) operations must cease because of labor availability or external conditions (weather, although external protection can be constructed around the printer), 2) process degradation (material consistency changing with time requires a process reset, or equipment breakdown occurs), or 3) the material is not strong or stiff enough to maintain the vertical building rate, and a pause is required to await hydration. As these pauses tend to occur in regular height intervals, usually at heights of approximately 0.5 m, the most likely explanation is the third one – that the material is just not able to go beyond this "buildability" limit, although process degradation is also a strong possibility. Whatever the case, scaling up continuous printing in space to larger print areas also involves scaling up in time to extended printing times, and current systems are apparently incapable of achieving this from a material or a process standpoint.

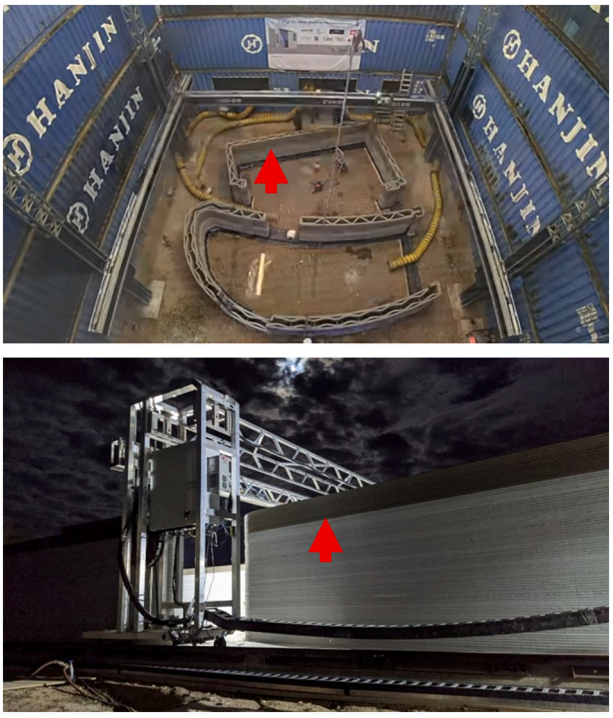

Fig. 3. Screen capture of Kamp C building production by COBOD printer in 2020 (a) [76] and military barracks in production by ICON printer in 2021 (b) [77]. The interface where production was stopped is clearly seen in both pictures, marked by a red arrow. (For interpretation of the references to colour in this figure legend, the reader is referred to the web version of this article.)

3. Analysis of the digital concrete extrusion processes: maximum vertical build rate for continuous printing

We now analyze the digital concrete extrusion processes to try and understand why large scale systems are primarily 1K, keeping in mind the possibility of reaching the industry benchmark of printing an entire building's vertical structures within a day. Roughly speaking, a 3 m high structure must be continuously printed at a rate of about 20 cm/h for 24 h.

Successful extrusion based 3D concrete printing has been based primarily on the strength buildup curve [36,50,78–80], which defines the material's tendency to collapse during production, aka the "buildability", in the terminology of the community. Collapse can occur one of two ways: either through plastic (strength based) failure, or elastic (stability based) failure [27,36,44,50,81,82]. In the former case, the height of the structure outstrips the ability of the bottom layer to support it, and in the latter case, the stiffness of the structure is unable to maintain its stability at a particular height and geometry, and it buckles and collapses. Strength-based failure can also be related to deformation-based failure, where pre-critical deformations can lead to failure to meet print requirements [44]. In all cases, to avoid failure, strength or stiffness must evolve with increasing height, although strength must evolve linearly while stiffness must evolve exponentially (to the third power) [27,44,50,82].

The strength of a cementitious material generally has two zones of evolution – during the dormant period when it is still workable, strength evolves primarily through interparticle interactions, and low-level hydration, which has commonly been called "thixotropy" within the community [83] (although differing somewhat from the more conventional rheological definition [84]). The onset of the acceleration period, where massive hydration begins to take place, marks the start of an exponential increase in strength and stiffness. In the literature, vertical building rates for extrusion based printing have generally been defined

Table 1
Various concrete 3D printing systems with some relevant capabilities.

Type	System	Type	Print area (m^2)	D_{max} (mm)	Processing rate (L/min)	Continuous printing, $H_{max} > 2$ m
1K	COBOD [21]	Gantry	14.5 m × unlimited	10	Up to 60	No
	ICON [65]	Gantry	8.5 m × unlimited	2	15	No
	USACE [20]	Gantry	120	9.5	15	No
	TU/e [1]	Gantry	40.5	1	3	No
	Loughborough [66,67]	Gantry	24	2	0.6	No
	Cybe [68]	Robot arm	<10	<4	~2–5	Yes
	NTU [69]	Robot arm	<10	<4	~1.5	Yes
2K	Sika [70]	Gantry	<10[a]	<4	15	Yes
	Baumit [71]	Robot arm	<10	<4	~1.5	Yes
	XTReeE [28]	Robot arm	<10	0.5	~1	Yes
	ETHZ [72,73]	Robot arm	<10	2	1.5	Yes
	DTI [19]	Robot arm	<10	8	2–5	Yes
	Ghent [49]	Robot arm	<10	1	6	Yes

[a] The Sika system is advertised as "up to 5 m" but does not specify which dimensions, so is possibly 25 m^2. This estimation is based on typical printed component sizes from Sika printers.

as the rate of strength gain within the first zone, usually given the terminology A_{thix} [50,78,79]. While buildability models generally predict failure based on this parameter (as well as the initial yield stress), it has been pointed out that the maximum attainable height based on thixotropy is limited – thixotropy in printable materials usually does not allow for much more than 10–30 kPa in strength [79], which roughly corresponds, coincidentally, to the height at which large scale 1 K systems stop printing (approx.. 0.5–0.75 m), as was pointed out earlier.

In Fig. 4, a strength buildup curve is shown that illustrates this. The point t_0 marks the time that water is mixed in with the cement and other dry materials – at this point, the clock begins towards the onset of the acceleration period and setting, defined by the open time, t_{open}. After placement of an extruded filament at t_{ext}, the material has some initial yield stress (or rapidly evolving "reflocculation" thixotropy, as described by Kruger et al. [80]) and its strength at rest begins to evolve at a rate of A_{thix}. As long as the load imposed by the vertical building rate does not exceed the maximum height of material the filament can withstand, then the continuous printing process will be successful. What can be seen in the figure is that if the height does not exceed a maximum height attainable from thixotropy before the onset of massive hydration, then the true maximum build rate for continuous printing can be given based on a criteria set by the open time and the "thixotropic maximum", $H_{max,thix}$ at the onset of the acceleration period. However, as can be seen in Fig. 1, each processing step up to the point of extrusion has its own residence time, which can be subtracted from the open time to shorten the time from extrusion to the acceleration period. Thus, the maximum vertical build rate for continuous printing in a 1K system can be estimated as:

$$\dot{h}_{max} = \frac{H_{max,thix}}{t_{open} - \sum t_R} \tag{2}$$

This analysis and expression can in part be attributed to an extension of the work in [78]. Given the above expression, one could also theoretically calculate the minimum contour length that could be printed continuously to structural scales, if one considers that $\dot{h}_{max} = \frac{hV}{L_{min}}$:

$$L_{min} = \frac{hV}{H_{max,thix}}\left(t_{open} - \sum t_R\right) \tag{3}$$

where h is the layer height and V is the printhead velocity. This gives an estimation of the point at which one should transition from a 1K system in which open time is managed, to a 2K system, based solely on avoiding plastic collapse.

Based on evidence seen in large scale 1K systems, where printing tends to stop at around 0.5–0.75 m, and given typical open times of 2–4 h, this means that maximum vertical building rates could be in the range of 12 cm/h to 50 cm/h without considering the pre-extrusion residence times, which can obviously shorten this quite significantly. There is even the possibility to significantly shorten the open time by using a fast setting cement and retarders, as is often done in quick setting CSA systems for pavements [85]. In any case, this clearly overlaps the 20 cm/h benchmark for 24 h building printing. Also, given normal layer heights of 1–2 cm and printhead velocities of 50–100 cm/s [21,65] this gives minimum contour lengths in the range of 50–400 m. At building scales, contour lengths are typically >100 m, so within this crossover range, this implies that longer contour length buildings should be able to be printed "in one go" with 1K systems, based on strength criteria. Does this mean that the apparent industry benchmark of printing an entire building's vertical walls within 24 h can be met?

It can be that it is not possible to meet the requirements imposed by stiffness evolution. As discussed earlier, Roussel [50] and others [44,82,86] have pointed out that buckling failure dominates at larger build heights, depending on geometry, and that the required elastic modulus increases with the third power of the height. Roussel gave a rough estimation using typical print material properties to give the height at which buckling failure dominates over a strength-based failure, based on critical strain. They concluded that at all reasonable critical strains, buckling failure will dominate for a 20 cm thick, 3 m high wall. Mechtcherine et al. [27] gives simple calculation criteria for strength evolution vs. elastic modulus evolution. To meet the benchmark of continuously printing a 20 cm thick, 3 m high wall within 24 h (density of 2000 kg/m^3) the linear strength evolution must be 0.4 Pa/s, while the linear elastic modulus evolution must be 230 Pa/s. Printable mortars are easily in the range of strength evolution of 3–4 Pa/s, but are usually (pre-setting) in the range of about 20–50 Pa/s for their modulus evolution [36,87]. The only way that this rapid evolution of elastic modulus can occur is through the massive formation of hydration products. This all suggests that elastic failure rather than strength-based failure sets the limit for continuous, wide area structural scale printing. In any case, the controlled onset of rapid hydration product formation after extrusion seems imperative after the transition from strength-based failure to elastic failure. Bos et al. [88] measured four different printable mixes which seems to illustrate this point: the most "buildable" mix (made with a rapid setting cement) showed a transition to a modulus evolution of 600 Pa/s after 30 min, which indicates that this mix should be a candidate for meeting the 24 h benchmark.

The fact that there seems not yet to be any industrial examples of a wide area structural scale, 1K continuous print implies that open time

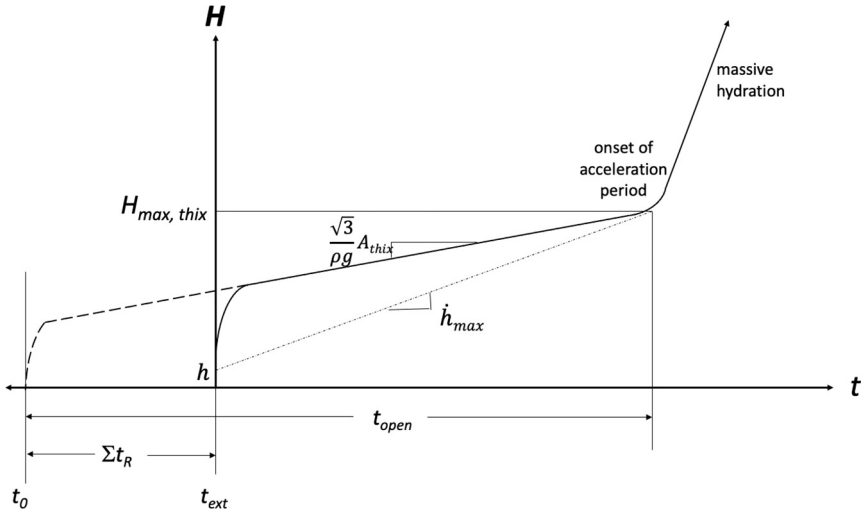

Fig. 4. Schematic of strength-based curve for continuous printing to structural heights. True maximum vertical building rate is determined primarily by the time from extrusion to the onset of massive hydration.

management must be difficult to manage at larger area scales and over the extended printing times required. It is necessary to avoid process deterioration caused by premature hardening in the processing line from primary mixing to extrusion, as was pointed out earlier. The longest residence times would tend to be the storage step, which often includes a hopper feed into a pumping device, and the pumping line itself. Residence times in each of these steps are not necessarily constant – Reiter et al. [61] pointed out that long pumping lines with fluid, accelerated material would inevitably lead to hardening due to the residence time distribution, which resembles that of a laminar flow reactor. One could imagine that reducing the size of the shear zone in the flow (i.e. increasing the yield stress and making it more plug flow) helps to mitigate this issue, however this may lead to more pumping difficulties. Gravity operated hoppers that feed typical pumping systems also potentially show broad residence time distributions, as analyses of granular feeding systems in the pharmaceutical industry, which operate under a similar principle, have shown [89,90]. A gravity operated hopper for a reactive yield stress fluid would probably also show a similarly broad distribution of residence times, although vibration can certainly help to mitigate this. In any case, the management of residence times to print continuously would be problematic primarily when the sum of the pre-extrusion residence times approaches the open time, and the total process time is extended beyond the open time.

The issue of processes changing over time can couple with this as a likely reason for the inability to continuously print. Wolfs et al. [87] indicated a change in early age structural properties as measured by ultrasonic pulse velocity measurements from start to finish of the process, where an increase in the buildup rate at the end of the process was attributed to heating from the pumping process. Diggs-McGee et al. [14] reported similar issues, even scheduling preventive maintenance to avoid buildup of concrete in the delivery lines. Most printing processes utilize a rotor/stator (progressive cavity) configuration for pumping, in which all heat generated during the pumping process is carried by the material, which undoubtedly causes a change in material open time during production, and complicates the issue of open time vs. residence time management. The issue of temperature also highlights the difficulty in properly handling the open time in hotter and colder climates, as well.

Thus, returning to the question of 1K systems and continuous vertical printing, indeed, shorter processing lines have been successful. Cybe's apparently 1 K robotic arm system is claimed to be able to print at fast vertical building rates, thanks to a mortar that sets in 3 min and gains structural strength in 1 h [68]. The NTU team in Singapore has claimed to have printed a structural scale (>2 m) prefabricated bathroom unit within 6 h, using again a robotic arm 1K system [69]. This seems to point out that managing the residence times and hardening rate between activation and extrusion is the primary key to being able to print at high vertical building rates at all scales, and that this is what is holding the industry back at larger scales. The most effective way to manage these residence times and control strength buildup is through the initiation of hydration in a “sleeping” (long open time) concrete as close to the point of extrusion as possible through the secondary (or inline) mixing step [61,91].

4. Secondary mixing: reactor design

The secondary mixer is of critical importance for accelerated digital concretes and mortars, not only for the reasons argued until now, but also because it forms the bulk of the printhead mass. Minimizing printhead mass must be a goal of any process and reactor design, as robotic arms and gantry systems have specified weight limits, and too large or bulky printheads can limit maximum speeds.

The role of the secondary mixing unit, indeed of any mixing process, is to reduce the scale of heterogeneity to an adequate level, which is defined for the process in question – in this case, the dispersion of a reactant into a bulk volume. For digital concrete processes, this required reduction of heterogeneity is sometimes given as a diffusion length scale estimated to be on the order of a few hundred microns [27,39].

The design of the secondary mixing unit is fortunately not a completely new undertaking, and the chemical processing industries offer vast amounts of literature for very similar problems to take inspiration from. In the following, a logical design sequence is presented in the determination of critical design parameters for an active mixing printhead unit. It is noted that a similar design sequence can be employed for static mixers, which have also seen some development for cementitious materials [45]. However, active secondary mixing units are currently far more reliable and flexible, and remain the state of the art in the growing 3D concrete printing industry, as evidenced by the only 3 printers on the market that are capable of printhead acceleration (XTReeE, Sika, and Baumit [70,71,92]).

Fig. 5 defines schematically an active mixing printhead unit. A reaction (mixing) volume V has a flowrate $Q_{C,in}$ of an inactivated concrete, to which a small volume of accelerator $Q_{A,in}$ is added, with an outflow of Q_{out}, which we designate as Q. A motor in the active mixing unit turns an impeller with a diameter D at a rotational speed of N. Typically, $Q_{C,in} \gg Q_{A,in}$ and flows in and out of the reactor can be reduced to Q; the volume being held constant in the reactor, we have that $Q_{C,\,in} + Q_{A,\,in} = Q_{out}$. The diameter of the impeller is generally on the same order as that of the reactor for yield stress fluids such as cementitious materials.

4.1. Inline mixer sizing

As pointed out earlier, the residence time of a reactor t_R is the average time a fluid element spends in the reactor, defined as

$$t_R = \frac{V}{Q} \tag{4}$$

Thus, sizing a reaction vessel volume V requires a processing flowrate and a residence time.

The homogenization number Ho is a dimensionless number defining the number of impeller revolutions to create a homogeneous mix [93,94]. It is sometimes called the mixing number N_{mix}, or the dimensionless blend time. This notation should not be confused with the rotation rate N, so we refer only to the homogenization number Ho for this parameter. Thus, the blend time t_{blend} (the amount of time required in the mixer to create a homogeneous mix) is defined as the ratio between the homogenization number and the rotational rate:

$$t_{blend} = \frac{Ho}{N} \tag{5}$$

The blend time is often reported as t_{95}, or the time required to reach 95% homogeneity (degree of mixing) defined by the coefficient of variance of a tracer concentration taken at various points [24,95].

For the mixing to be effective, the fluid must remain in the mixing

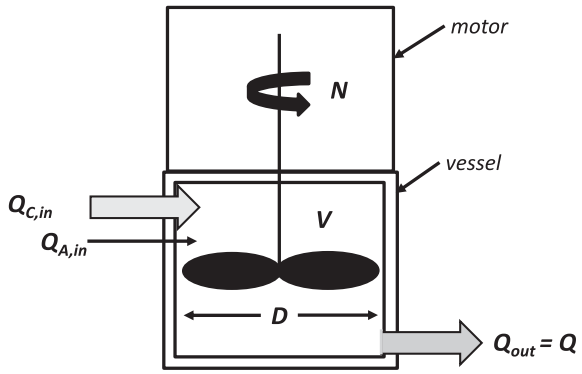

Fig. 5. Inline mixer (reactor) schematic. An inactivated concrete is pumped with an activator into an active mixing vessel of volume V, as a motor turns an impeller of diameter D at speed N. As the volumetric flowrate of the activator is small, the overall flowrate into and out of the volume is specified as Q.

volume long enough to be adequately mixed, but it must not remain so long that it begins to harden unacceptably, leading to process degradation, difficulty in extruding, blockage, or cold joints. Thus, an upper time limit has to be defined based on the hardening characteristics of the activated material, which we define as t_{act}, or activation time. The residence time thus must fall between the blend time and the activation time:

$$t_{blend} < t_R < t_{act} \tag{6}$$

The activation time can be thought of as the time the material needs to achieve a particular strength τ_{max} above which it no longer meets process requirements, which can vary by system and depends on the strength buildup model. This can be related to linear strength buildup via the following relation:

$$t_{act} = \frac{\tau_{max} - \tau_0}{A_{acc}} \tag{7}$$

where A_{acc} defines a linear strength buildup rate after acceleration, similar to A_{thix}, and τ_0 is the initial yield stress. While t_{act} could be defined by more complicated models, here we use the linear model for simplicity. Combining (4), (5) and (7) with (6), we then have an upper and a lower limit defined for the reactor volume based on process and material parameters:

$$\frac{QHo}{N} < V < Q\frac{\tau_{max} - \tau_0}{A_{acc}} \tag{8}$$

Process flowrates are generally dictated by the pumping equipment and printhead velocity to achieve a particular production rate so that a particular filament cross section can be achieved that meets specifications regarding shape, buildability and cold joint formation [2,27,50,79]. The homogenization number Ho is generally a function of impeller and reactor geometry, and is influenced by the mixing Reynolds number Re_m. The accelerated strength buildup rate (and activation time) is primarily determined by material parameters, especially the accelerator reaction rate and dosage, and how they change the strength buildup curve. Therefore, for a specified flowrate, one can dimension a reactor's residence time to fit within this window through the homogenization number, the impeller speed and geometry, and the accelerator type and dosage. This is depicted schematically in Fig. 6.

It is worth going into more detail regarding the accelerator types, the Reynolds number, and the homogenization number, as they relate to reactor design.

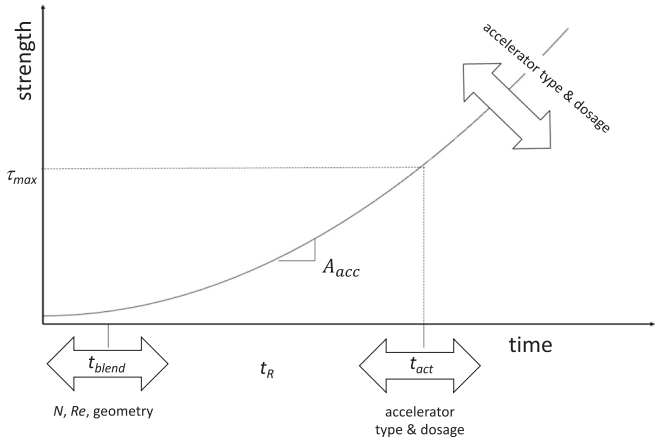

Fig. 6. Strength buildup curve schematic for a secondary mixing unit operation. The residence time must be greater than the blend time, but less than an activation time, and strength buildup rate is determined primarily by accelerator type and dosage.

4.1.1. Accelerator type (reaction rate)

Accelerator types play a large role because they dictate the strength buildup curve – a fast-acting accelerator will thus tend to require a short residence time before deposition, and a slow one will require a longer residence time. When looking at Fig. 6, one can see that the accelerator type plays a large role on A_{acc} and thus t_{act}, or the upper bound of the residence time. The experience of the authors has shown that commercially available accelerators acting primarily on the main hydration peak, such as C-S-H seeds or calcium nitrate-based accelerators, require at least 30–40 min before they build strength appreciably [46,51]. These have been described using an exponential relationship in strength buildup to account for the very slow buildup in the beginning [96].

Set accelerators relying on ettringite precipitation, such as calcium aluminate cement (CAC) or calcium sulfoaluminate cement (CSA) additions (typically 5–10% OPC substitution), or alkali-free shotcrete accelerators such as those based on aluminum sulfate (typically 2.5–4% by weight of cement), begin to build strength within seconds to minutes after addition and thus are more suitable for shorter residence times [44,45,97]. Indeed, studies indicate that typical strength buildup rates for CAC-based acceleration is in the range of 1000 Pa/min [44], while for aluminum sulfate based solutions it is higher at 2000–3000 Pa/min, although better approximated with a power law [47]. The upper limit of yield stress will be dependent on the system and material in question, but may in first approximation be estimated as equivalent to that of a near-zero slump yield stress (about 3000 Pa). This makes for typical activation times for these accelerators somewhere in the range of 50–150 s. It should be noted, however, that these strength buildup rates are based on small area contours, and that it is probable that the accelerator dosage (and the strength buildup rate) can be significantly reduced for larger area contours, so there may be more play with this parameter even with fast acting accelerators.

Most successful commercial and academic digital concrete processes employ the solution of using fast acting accelerators, although the use of slower acting accelerators is a viable solution for large print areas with long contours. Indeed, if one considers Fig. 4 and Eq. (2), one can replace the denominator with the post acceleration open time to determine the new maximum build rate.

4.1.2. Reynolds number

The impeller Reynolds number (also called the mixing Reynolds number, Re_m) plays a critical role in the design of any active mixing operation. It is defined by:

$$Re_m = \frac{\rho D^2 N}{\mu} \tag{9}$$

where ρ is the material density, D is the impeller diameter, N is the impeller rotational speed, and μ is the material viscosity. The mixing Reynolds number determines the flow regime, which determines the primary mixing mechanism. A mixing Reynolds number on the order of 10–20 and below is considered as laminar flow where stretching and folding of fluid layers dominates as a mixing mechanism. Above about 10^3 is considered fully turbulent, where tumbling and retumbling of eddies across various scales dominates mixing, and the behavior between both limits is transitional, where a mixture of mechanisms is determined to be involved [24,93,94,98]. While the majority of mixing in the chemical processing industries is turbulent, in digital concrete processes, it is almost exclusively laminar due to the high viscosities of these dense solid suspensions, although transitional flows can likely be accessed if the viscosity is low enough, as described later. As a real-world example, the ETH Zurich 3D printing platform [72,73] has a diameter of approximately 7 cm and a speed of 125 RPM. Therefore, given a density of 2000 kg/m^3 and an estimated viscosity of about 1–5 Pa·s for the printable mortar, Re_m is in the range of 4 to 20. When one considers that the viscosities of very fluid grouts and mortars can be as low as 0.1 Pa·s, then Re_m can be in the range of hundreds, and thus

within the transitional regime. High concrete viscosities (order of magnitude tens of Pa·s) clearly place coarse aggregate mixes in the laminar regime [99].

4.1.3. Homogenization number

The homogenization number *Ho*, representing the number of revolutions to create a homogeneous mix, is a dimensionless number that depends primarily on impeller geometry and the mixing Reynolds number. Much experimental data has been published on the relationship of this number to various parameters [24,93,94], and it has been suggested that generally, it is roughly constant in the laminar and turbulent regimes while varying in the transitional regime [24], which is seen in Fig. 7. This figure also shows experimental data on helical ribbon impellers (a close-clearance impeller normally used for yield stress fluids) showing that *Ho* can vary between 20 and 300 for this geometry, depending on the flow regime [100]. Most interestingly, *Ho* increases significantly in the transitional regime in this experimental data set, highlighting the importance of knowing which flow regime a given design will occupy. In the case of the ETH Zurich 3D printing platform used for the Concrete Choreography project [72,73], the volume is around 0.6 L, the speed is 125 RPM, and the processing flowrate typically around 1.5 L/min, which gives an estimated *Ho* around 50, assuming that this process is running at its homogenization lower limit at this flowrate.

4.2. Mixing power analysis

While the previous analysis gives an idea of how to size the inline mixer, it is equally important to analyze the required power for mixing in order to adequately dimension the motor. Generally, in the processing

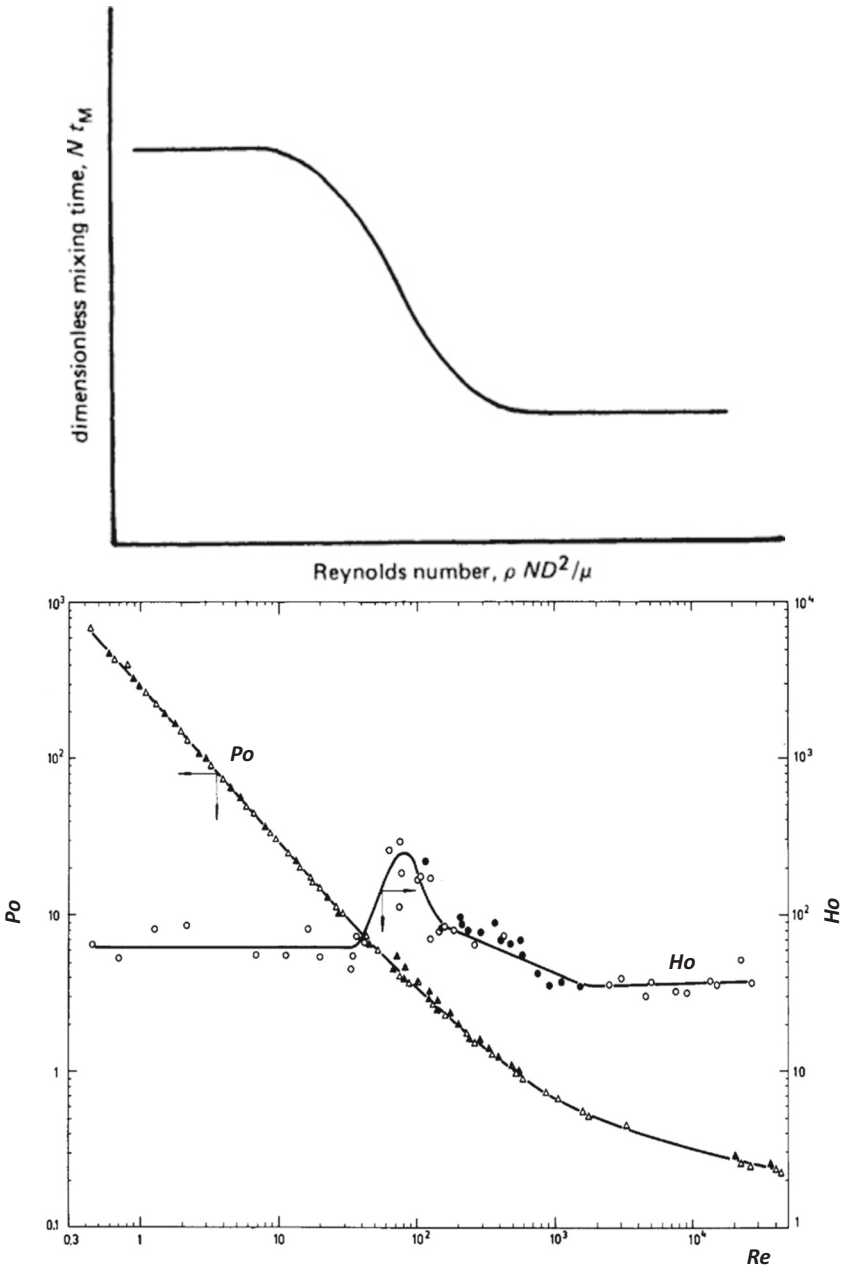

Fig. 7. (a) Schematic showing general dimensionless blend time behavior versus flow regime of impeller Reynolds number Re_m, from [24]. (b) Experimental data of homogenization number *Ho* vs impeller Reynolds number as well as Power number *Po* vs. impeller Reynolds number, taken for helical ribbon impellers [100]. Figures obtained with permission from the respective references.

industries, it is aimed to minimize the required power to minimize costs for continuous operation. In digital concrete processes, this should also be an aim, not only to minimize costs, but to minimize mass on the printhead.

Besides the Reynolds number, the Power number *Po* (sometimes called the Newton number *Ne*) is an equally critical number in mixing process analysis [23–25,93,94,101]:

$$Po = \frac{P}{\rho N^3 D^5} \tag{10}$$

where P is the power applied to the impeller, ρ is the fluid density, and N and D are the impeller speed and diameter, respectively. While the Reynolds number is the ratio of inertial to viscous forces in the fluid, the Power number is a dimensionless number that can be thought of as a ratio between the drag force and the inertial force of the impeller, and that is dependent on the impeller geometry [98].

In the laminar mixing regime ($Re_m < 20$), the quantity $PoRe_m$ is constant, meaning that the power scales with Re_m^{-1} giving

$$P = K_P \mu N^2 D^3 \tag{11}$$

where one can see that mixing power depends on fluid viscosity. The constant K_P is a constant of proportionality equal to $PoRe_m$, and thus is also a function of the impeller's geometry, with many correlations existing in the literature [23,93]. It is also sometimes referred to as the *laminar power constant*. When plotted on a log-log scale, the Power number and the Reynolds number show a linear relationship with a slope of −1, as expected based on their inverse relationship and seen in Fig. 7 and Fig. 8.

In the turbulent mixing regime ($Re_m > 10{,}000$), the mixing power is independent of the Reynolds number as inertial forces dominate and the following relationship holds from (10):

$$P = Po\ \rho N^3 D^5 \tag{12}$$

In the transitional mixing regime ($10 < Re_m < 10000$), while power correlations vary with impeller type, the Power number does show a weaker dependence on the Reynolds number [98]. Some authors have stated that power scales with $Re^{-1/3}$ [94], which would give the following relation:

$$P = Po\ \rho^{2/3} \mu^{1/3} N^{8/3} D^{13/3} \tag{13}$$

Thus, power is dependent on both the fluid density and the viscosity in the transitional regime. Fig. 8 shows how mixing power in general is related to Reynolds number through the various regimes. Clearly, of most interest in the digital concrete community will be the laminar and transition regimes, as stated before. For the rest of the analysis and for simplicity, we focus primarily on laminar mixing with the knowledge that transition flows in the applications considered will likely be rare and turbulence nonexistent.

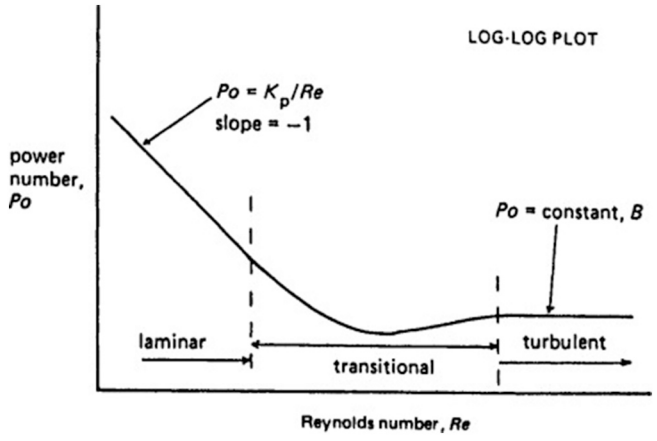

Fig. 8. Variation of Power number with Reynolds number for mechanically stirred systems. Figure taken with permission from [24].

One can see from (11) that for laminar mixing, finding the constant K_P will allow for the calculation of the power requirement for mixing in a given geometry, speed, and viscosity. This constant can be estimated by measuring the power (or torque) of a mixer at a given speed, and is dependent primarily on the geometry of the impeller. For the ETH Zurich printing system, an impeller power has not been measured for the given material system, so a best guess estimation is made with measurements using the Pheso concrete rheometer [102,103], which has an impeller geometry of multiple pins similar to that of the ETH Zurich printing system. The measurements undertaken are given in Supplementary Information SI-I, and return a K_P of 600, which serves as our estimation for the print system impeller. This is quite reasonable considering other close clearance impeller geometries, such as double helixes or anchors, have K_P values on the order of 300–500 [93].

5. Printhead scaleup

Scaleup is a common procedure in the chemical processing industries, in which a pilot or lab sized unit operation is then used as a model for production level. It requires the translation of the essential parts of the process at the larger scale. For the secondary mixing unit operation of 2K digital concrete processes, scaleup means, generally, increases in dimension, at least enough to accommodate larger aggregates, and almost certainly an increase in flowrate. According to Table 1, there should be a flow rate increase up to 5–30 fold if current 1K processes transition to 2K. Both these increases in dimension and flow rate will certainly require an increase in reactor mass. However, as previously mentioned, the mass of a moving printhead, which includes the reactor, should be minimized, which the following analysis examines.

The mass of a printhead with an inline active mixer for digital concrete will be the sum of three major parts: the concrete mass, the mass of the reactor vessel to hold the concrete, and the mass of the motor and impeller.

$$M_{printhead} = m_{concrete} + m_{vessel} + m_{motor} \tag{14}$$

Clearly, concrete mass scales with the density of the concrete and the volume of concrete in the vessel:

$$m_{concrete} = \rho_{concrete} V \tag{15}$$

The mass of the reactor vessel is expected to scale linearly with the volume of concrete in the vessel as well. Included in this is the mass of the impeller. The impeller design will be dominated by the mixing process, but its mass will scale with the anticipated mechanical forces. The vessel design will be determined primarily by considerations of expected mechanical forces, pressures, resistance to the alkalinity of concrete, and ease of assembly and cleaning. For the purposes of this analysis, a simple linear relationship is proposed below:

$$m_{vessel} = c_{m,vessel} V \tag{16}$$

where $c_{m,vessel}$ is a scaling constant relating the mass of the vessel components to the volume of concrete in the reactor. The ETH Zurich printhead is a prototype and it is difficult to estimate a useful constant from its mass. Thus, a first estimation can be made from standard concrete mixers, and is estimated at 4000 kg/m^3 concrete (see Supplemental Information SI-II). One should keep in mind this is an estimation that can vary widely based on material selection and design, as discussed later in Section 6.

The mass of the motor is expected to scale linearly with its power, based on previous studies on the subject [104,105]. Generally, motors also include gearboxes which would scale similarly. The motor mass would then be expected to follow the relation:

$$m_{motor} = c_{m,P0} + c_{m,P}P \tag{17}$$

where $c_{m,P0}$ is a minimum motor weight required, and $c_{m,P}$ is a constant relating the motor mass to its power. The data for some motors in the range 0.1–0.9 kW from the motor company TEC are taken as a reference (see Supplementary Information SI-III). They give a $c_{m,P}$ of 0.005 kg/W, and a $c_{m,P0}$ of 2.5 kg. This is well within the range of common weight to power ratios, which go from 0.003–0.01 kg/W for electric motors.

If one combines (11) with (14)–(17), and considers that D^3 is related to the reactor volume and can be replaced by V, one obtains the printhead mass scaling relationship for laminar mixing:

$$M_{printhead} = \left(\rho_{concrete} + c_{m,vessel} + c_{m,P}\, K_P\, \mu N^2\right) V + c_{m,P0} \tag{18}$$

where one can see that the printhead mass is composed of 3 parts, all which scale proportionally to the reactor volume if all other parameters are held constant. The motor mass can be thought of as a mass required to provide a particular power per unit volume. Scaleup would allow for the adjustment of two parameters: the volume V in case of an increase in linear dimension, or the speed N in the case of increasing mixing power. In the following, two cases of scaleup are analyzed:

1) keeping speed N constant and increasing V, and
2) keeping V constant while increasing N.

In terms of digital fabrication with concrete, the first situation would be required in the case of an increase in maximum aggregate size, while both scenarios could be utilized to accommodate the increased flowrates expected for upscaling active mixing printheads for digital concrete. Table 2 gives an estimation of some parameters based on the ETH Zurich 3D printing setup and constants estimated as noted previously.

5.1. Constant speed

We first consider the case of keeping the impeller speed (N) and geometry (K_P) constant and simply increasing the volume V. The three terms in the brackets of (18) are constant, so that the total printhead mass increases linearly with V. This increase in volume can be a result of either a required increase in dimension, to accommodate either larger aggregates or an increase in flowrate Q. Using constants and parameters from Table 2, Fig. 9 can be generated showing the proportional increase of each printhead component with increasing volume.

The vessel components clearly dominate the mass of the printhead, and the required motor mass contributes negligibly as volume increases. This, however, is highly dependent on $c_{,m,vessel}$, which in this case is approximately double the density of concrete. Clearly, there are some possibilities to optimize this, which will be discussed later in Section 6.

5.2. Constant volume

If one is scaling up by increasing the flowrate Q, one can also maintain a constant volume and increase the speed N to deliver the required power per unit volume to ensure a homogeneous mix. To accommodate an increase in flowrate, it is more convenient to look at (18) in terms of Q by substituting in QHo/N for V:

Table 2
Scaling parameters based on ETH Zurich printing setup. Mass and laminar power constant estimations given in Supplementary information.

$\rho_{concrete}$	$c_{m,vessel}$	$c_{m,P}$	$c_{m,p0}$	μ	Ho	$K_P = PoRe_m$	N	D
kg/m^3	kg/m^3 concrete	kg/W	kg/W	Pa·s	rev	–	rev/s	m
2000	4000	0.005	2.5	1	50	600	2	0.07

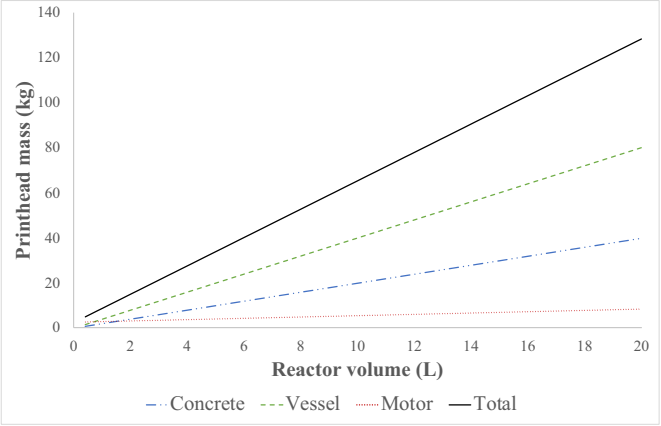

Fig. 9. Estimated printhead mass vs. reactor volume of concrete for ETH system (values from Table 2).

$$M_{printhead} = \left(\rho_{concrete} + c_{m,vessel} + c_{m,P}\, K_P\, \mu N^2\right) \frac{QHo}{N} + c_{m,P0} \tag{19}$$

which is the same as stating that the blend time is equal to the residence time and corresponds to the lower limit printhead size.

In Fig. 10a, one can see how the estimated mass of the printhead remains very low using this approach (discontinuous line) compared to increasing the volume of the mixer (continuous line), even at high flowrates. This is rather surprising, considering the N^2 dependence of the third term in (18). In any case, this finding implies that, when scaling up to higher flow rates, one should increase mixing speeds rather than the reactor volume.

However, when one examines Fig. 10 (bottom), which shows how varying the viscosity of the material can change the curve, one can see clearly that with increasing viscosity, there is a faster increase in printhead mass when one simply increases the mixing speed to deal with an increase in flowrate. The curves in Fig. 10 are really meant to be indicative, because for the case considered, the rotational speeds start to become unrealistically high – at a flowrate of 40 L/min with a reactor volume of approximately a half liter, the residence time is 0.75 s and the required speed would need to be more than 4000 rpm. With a viscosity of 50 Pa·s, the calculated power is very high, in the range of 67 kW. It is clear, however, that the viscosity plays a major role in the mixing power, which is of prime importance for upscaling to larger aggregates and can increase the viscosity by an order of magnitude or more. A good grading of the aggregates therefore plays an increasingly important role for scaling up extrusion printing.

5.3. Scaleup in the digital concrete processes

The previous two analyses just manipulate the two primary parameters to ensure adequate mixing (speed and volume). Scaling up however often involves the adjustment of both. It also usually deals with the same material, but in this case of interest to this paper, we scale up to concrete with coarser aggregates, which can significantly increase viscosity and this must be taken into account.

The goal of scaleup in the digital concrete processes must be to meet process requirements at a minimal printhead mass. One can see that increasing impeller speed leads to very high power requirements, and a much heavier motor, especially with an increasing viscosity. Thus, when scaling up to larger aggregate sizes, it is probably best to scale up by increasing reactor volume enough to maintain a low enough impeller speed. However, when scaling up to increase flowrates, if viscosities are low, then simply increasing motor speed may be sufficient. This requires, however, a very effective mixing geometry, which also means that having low viscosities is extraordinarily helpful in keeping

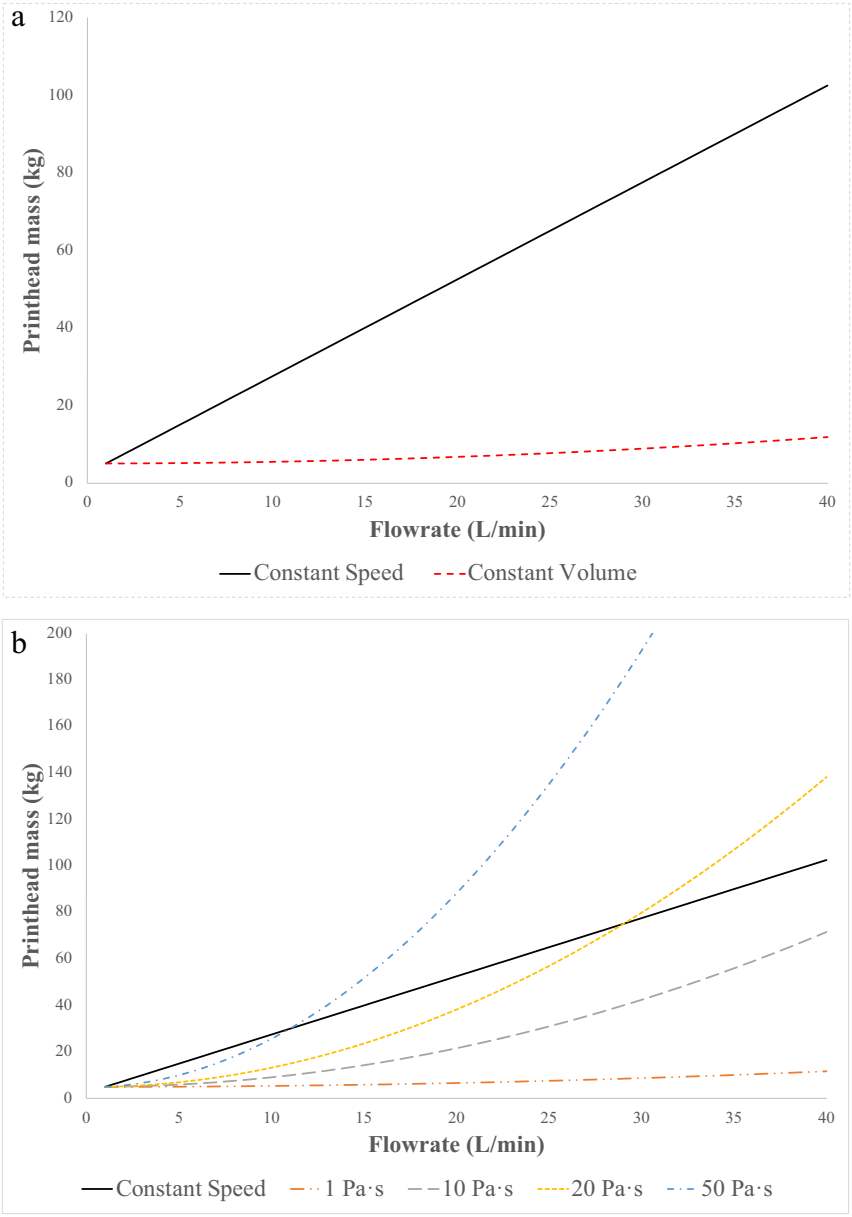

Fig. 10. (a) Comparison of printhead mass increase to accommodate higher flowrates by increasing mixing speed or increasing mixer volume for ETH mix (parameters taken from Table 2). (b) Graph showing how increasing viscosities alters the picture for this system by drastically increasing power, and thus motor mass, requirements. Original viscosity is 1 Pa·s.

equipment requirements to a minimum.

It is also absolutely essential to understand the flow regime that the process occupies. For example, if by scaling up a process, the regime changes from laminar to transitional (or vice versa) the mixing behavior and power requirement can change significantly. Generally, digital concrete processes are laminar and do not run this risk, except in the case of high speed and low viscosity processing.

One important thing to note as a primary principle in scaling has to do with geometric similarity. In general, one has a good chance of maintaining process performance if geometric similarity is maintained from a prototype to an upscaled unit operation, and the work required is lessened [93,98]. Scaling up geometrically dissimilar systems is of course still possible, but one must really take geometric differences into account and understand the higher degree of difficulty in realizing process performance that can result from taking this approach. Non-geometric upscaling can also be necessary or even advantageous, depending on the aspect of the process which is most important [93]. What can be emphasized here is that gaining a greater understanding of the mixing process is essential to ensure scaleup success, regardless of the approach taken.

6. Discussion and practical considerations

Earlier in this article, we examined the steps in a digital concrete process from a process engineering standpoint. In particular, the focus on 1K vs 2K systems led to the conclusion that large area, continuous printing would benefit greatly from a transition to a 2K system with a secondary mixing unit operation. Inclusion of such a step makes it the critical stage that dictates many material requirements. We have then followed with an analysis of mixing from a process engineering standpoint, with a discussion of its implications for scaleup. The following discussion will now center on reactor design and other issues from a practical standpoint, based both on the literature and the authors' experiences.

6.1. Reactor (inline mixer) design

6.1.1. Size

As was discussed earlier, the required reactor volume must fit within the parameters set by Eqs. (8) or (6), in which the flowrate plays the critical part. The upper bound of the reactor size is established primarily by the material and process requirements for strength buildup (accelerator type and dosage), while the lower bound is established by the geometry and the impeller speed. The size, however, is also limited by robotic toolhead requirements, as robotic arms often have weight limits, and even gantry-based systems can be disadvantaged by heavy and bulky toolheads requiring more power and difficulties to move with the precision that the greater inertia demands.

6.1.2. Impeller

The impeller design should be dictated by the requirements of reaching proper blending at the lowest power input possible, meaning with a homogenization number *Ho* and Power number *Po* (or, rather the laminar power constant K_P) as low as possible. Cementitious materials are yield stress fluids with high viscosities, and this means that impellers should be close-clearance designs such as helical ribbons [98,106] or with some sort of scraper employed to ensure material does not channel by sticking close to the vessel wall. Impellers designed for powder processing such as for pin mixers are also recommended and have been used previously [44,72,73]. Good impeller design also dictates proper mechanical design of shaft and blades to resist shear, torsional, and bending stresses induced during operation, especially from the fatigue standpoint [107]. Blade design should promote slicing, reorientation and redistribution of fluid flows. Finally, the impeller and reactor volume should be designed such that dead zones are eliminated, but also that channeling is minimized, as stated earlier. The ability of the impeller to enhance pumping action can also be useful, especially to promote some degree of backmixing, but care should be taken with respect to how this impacts the residence time distribution.

6.1.3. Motor

Motors should be chosen to provide the required power per unit volume. This power is most dependent on the material viscosity, the impeller diameter, and the required speed, and can be calculated from (11) for the laminar flow regime. For most digital concrete processes, this will likely be in the range of a 0.1–5 kW. Motors with high power to weight ratios (or high power densities) should be favored to minimize the reactor volume and thereby the mass of the printhead. Electric motors are capable of high power to weight ratios, but the use of hydraulic motors, driven by circulating hydraulic fluid rather than electrical energy, may offer a useful solution to minimizing printhead mass and volume, given their power to weight ratio is up to an order of magnitude higher than electric motors [108].

6.1.4. Inlet

The inlet location is of critical importance. Especially in the case of highly reactive accelerators, the potential for clogging is very high so a constant positive pressure (provided by the accelerator dosing pump) is a must [73], combined with a scraper from the impeller close to the inlet to break up fast forming agglomerates. The inlet location should be chosen to allow for efficient reorientation of flows, with minimal chances of dead zones and channeling.

6.2. Materials

The mass constant $c_{m,vessel}$ in (18) forms a critical part of the mass of the printhead, so careful selection of materials combined with good mechanical design can go a long way to minimize that mass. For example, overdesigning mechanically can lead to unnecessary weight added to the printhead, and selection of higher density materials could also lead to increased printhead mass. It is important first, however, to select materials that are capable of withstanding the aggressive alkalinity of the cementitious pore solution, as well as materials that are capable of easy cleaning and maintenance. The materials should also be capable of withstanding the mechanical forces and abrasion brought by the process – this is particularly important in the case of the impeller, as well as the chamber in the case of pressurized systems. Stainless steel, and alkali resistant polymers are among the best choices for materials.

6.3. Material mix design

The mix design of the printable material is dictated primarily by end performance – the need for it to have adequate strength and durability during its service life, as well as the need for it to have adequate buildability during the production process. In the case of the secondary mixing step, it is essential to know the material behavior at potentially very high shear rates, so that the material can be adequately processed while still meeting these downstream requirements. Clearly, the materials should not be shear thickening, and ideally, they are shear thinning to reduce required power inputs. Well-designed materials with proper particle packing (well graded materials) should be a key goal, and the use of viscosity reducing admixtures can be potentially very useful in minimizing power requirements, and thus printhead mass. The 3d printing concrete industry has been trending towards drymix materials where effective control of the mix design is performed during the mix proportioning step to make processing much easier [70,109]. The move towards larger aggregates, and especially the most attractive option of using local materials, may complicate this strategy, but it is not an impossible task. However, it should be emphasized that the development of concentrated suspensions with a low viscosity is overall a very complex undertaking, which will pose challenges in many upstream process stages, requiring more precision and controls, especially in the dosing step. A final point can be made with respect to density of mix design – while viscosity reduction is a laudable goal for processing, lower density mix designs can also be useful towards that end as well. Lower densities, besides obviously enhancing buildability, correspond to lower mixing energies and lower energy dissipations, which are all useful for reduction of power requirements in the printhead. The potential tradeoff with strength, however, should be assessed.

The design of the accelerator is quite important as well, from both a chemical and physical standpoint. While fast acting accelerators are very useful for buildability in very rapid vertical building rate prints (1–8 m/h) with short contour lengths, a slower acting accelerator may be useful at the larger scales with longer contours and slower vertical buildup rates (0.2–0.5 m/h). The longer activation times of slower acting accelerators works in favor of the process in terms of implementation into a reactor where a longer residence time might be necessary or useful. Inducing strength buildup through hydration product formation rather than through the use of viscosity modifiers has been recommended earlier [44] for reasons of buildability, but is also important in the context of processing. Using viscosity modifying admixtures to enhance the initial yield stress runs the risk of requiring high power inputs in the mixing reactor due to the increase in viscosity [73]. Viscosity reduction during this critical step is a more useful process design goal, and some viscosity reducing admixtures, as stated before, can be useful towards this end. Thus, an effective admixture should reduce the viscosity at high shear, while providing some rapid structural build up at rest and being easily combined with an appropriately acting accelerator leading to hydrate precipitation at the required rates. A last comment on the accelerator design has to do with matching rheological parameters. The reactive dispersion of a small volume of material into a larger one can already be complex enough, but major viscosity differences between the accelerator and the concrete create even more difficulties, so it is advised to match rheologies as much as possible.

One aspect that is not well captured in the analysis of this paper is the shear rate dependence of viscosity. It is well known that cementitious materials are non Newtonian fluids, demonstrating Bingham or at least

yield stress behavior, and demonstrating either shear-thinning or shear thickening behavior at higher shear rates, depending on their composition and processing conditions [110]. To deal with non Newtonian fluids, the most common approach taken in the processing industries is that of Metzner and Otto [111–113]. They proposed the following empirical relationship to estimate an average shear rate (or effective shear rate, $\dot{\gamma}_{eff}$) for a particular impeller geometry:

$$\dot{\gamma}_{eff} = K_S N \tag{20}$$

where N is the impeller speed, and K_S is the Metzner-Otto constant, which is dependent on the impeller and vessel geometry. This relationship was originally developed for shear-thinning fluids, and it holds well in the laminar regime for a variety of impeller and tank geometries [113]. While it has successfully been used for decades in the laminar regime, in the transitional regime and beyond, it has been found not to be completely accurate. However, it can offer a good starting point for a more refined analysis as most digital concrete work is in the laminar mixing regime.

6.4. Current real world printheads

Concrete 3D printing systems show a variety of designs, and implementation of a secondary mixing process into them requires an understanding of other process demands that require equipment and design modifications on the toolhead as well. For example, an incredibly useful process feature is start/stop operation. Many systems, such as the USACE system, are usually controlling extrusion pressure from the pump to a passive printhead, and this severely limits geometric control in start/stop, which then dictates the print path to be as continuous as possible. The COBOD system [21] and the printhead developed by the ConPrint3D project [114], on the other hand, have a rotor/stator pump fed by a hopper directly on the printhead which controls the extrusion rate and pressure while giving very precise start/stop capabilities. However, this also significantly adds to the printhead mass and could complicate the implementation of a secondary mixing system. Inline mixing systems for these types of printheads could be impellers coupled to the rotor shaft, but in this case impeller speed is limited by extrusion rates. An impeller geometry that matches the homogenization number to the extrusion rate (and thus the rotational rate), however, is a potentially attractive possibility, but would require the measurement of the homogenization number and development of a proper geometry for consistent mixing. Motor size would be irrelevant, as power requirements for extrusion would be much more than mixing power. Another possibility would be to have motors not coupled to the rotor/stator axis, but driving impellers in another volume of the reactor. This adds extra motor mass and volume, obviously, but has the advantage of flexibility in speed.

Finally, the desire to implement many different functionalities on the printhead also plays a major role in printhead size. Reinforcement implementation directly from the printhead, for example the cable inlay system pioneered by TU Eindhoven [115], requires both mass and volume in the printhead. Other systems, such as finishing systems, also would cause the same issue to a lesser degree. A particularly novel approach, in which primary mixing is performed directly within the printhead, has even been demonstrated recently [116]. A large number of functionalities might, in fact, require a focus more on minimizing and optimizing volume rather than mass: printheads also have limited space within which to work, so design considerations may dictate selection of a high power density motor rather than a high power to weight ratio. However, current active commercial printhead designs have very limited functionalities, so this is just a consideration for the future, as the field develops.

7. Conclusions

This paper touches on a variety of topics, all related to the implementation of some process engineering principles in the production of 3d printed concrete structures. The primary conclusions are detailed below, with some considerations for future research highlighted.

A. 3DCP systems can be decomposed into their individual processing steps, and each step has its own residence time and RTD. The material and processing should be designed with consideration for the critical step, and in the case of 2K systems, this is the secondary mixing.
B. Large area systems with long contours are all 1K systems so far, and can theoretically allow for continuous printing to structural heights through adequate management of the open time during the process. However, this does not yet seem to have been realized, most likely because RTD management at extended processing times is difficult to control, while maintaining the timing of rapid evolution of hydration products that is required to avoid buckling failure.
C. Implementation of a 2K system, where an accelerator that initiates hydration product formation is intermixed just before placement, will greatly facilitate printing at the scale of a building within the 24 h benchmark. This will require, however, proper development of equipment and accelerator selection.
D. Effective printhead design requires an understanding and characterization of certain dimensionless numbers, such as the homogenization number *Ho*, the mixing Reynolds number Re_m, and the Power number *Po*, and all are well studied in the processing industries. All are linked to the impeller and reactor geometry, and the geometry should be chosen to minimize both *Ho* and *Po* at a particular Re_m.
E. The majority of the printhead's mass comes from the vessel materials at the relatively low viscosities for 2K systems. Increasing viscosity has a very large impact on the mass of the motor required in an active mixing printhead, especially as the mixing speed increases. This has large implications for scaling up to larger aggregates, which often involves a 10 fold or more increase in viscosity compared to mortars. Larger scales fortunately are typically gantry systems, which lend themselves better to heavier printheads.
F. Minimizing viscosities at high shear rates through the use of well-designed admixtures and optimized packing, in combination with a properly designed and dosed accelerator that induces adequate hydration product formation to avoid buckling failure will likely be the pathway to realizing the goal of a continuous, wide area print with coarse aggregates.
G. Determination of residence time distributions and homogenization numbers requires development of useful quantitative methods of analyzing mix homogeneity, such as using pigments or other tracer materials. These could then be related to a much easier to measure process parameter, such as yield stress.
H. True chemical reactor engineering can proceed when reaction rates of various accelerators can be more fundamentally linked to hydration product formation and evolution of rheological parameters, allowing more precise calculation and prediction of activation times for given processes.

CRediT authorship contribution statement

Timothy Wangler: Conceptualization, Methodology, Formal analysis, Investigation, Writing – Original Draft, Writing – Review & Editing, Visualization, Supervision.

Rafael Pileggi: Conceptualization, Methodology, Writing – Original Draft, Writing – Review & Editing, Visualization.

Seyma Gürel: Formal analysis, Investigation, Writing – Review &

Editing.

Robert J. Flatt: Writing – Review & Editing, Supervision, Funding acquisition.

Declaration of competing interest

The authors declare that they have no known competing financial interests or personal relationships that could have appeared to influence the work reported in this paper.

Acknowledgements

The authors would like to acknowledge the National Centre for Competence in Research – Digital Fabrication in Research (NCCR Digital Fabrication, Agreement # 51NF40-141853) from the Swiss National Science Foundation for funding support of Dr. Timothy Wangler and Seyma Gürel. The authors also acknowledge the ETH Zurich Department of Civil, Environmental and Geomatic Engineering for the visiting professorship of Dr. Rafael Pileggi at ETH Zurich.

The authors are grateful to Ana Anton and the Chair of Digital Building Technologies, Prof. Benjamin Dillenburger, for their cooperation in providing printhead dimensions and other important information used in this article, as well as valuable input during discussions. Dr. Lex Reiter, Dr. Ena Lloret-Fritschi, and Fabio Scotto are also acknowledged for their inputs in discussions and exchanges.

Philip Fleischmann, Michael Lyrenmann, Tobias Hartmann, Martin Keller, Andreas Reusser, and Heinz Richner are all acknowledged for providing valuable material, design, and process support.

Appendix A. Supplementary data

Supplementary data to this article can be found online at https://doi.org/10.1016/j.cemconres.2022.106782.

References

[1] F. Bos, R. Wolfs, Z. Ahmed, T. Salet, Additive manufacturing of concrete in construction: potentials and challenges of 3D concrete printing, Virtual Phys. Prototyp. 11 (2016) 209–225.
[2] R.A. Buswell, W.R.L. De Silva, S.Z. Jones, J. Dirrenberger, 3D printing using concrete extrusion: a roadmap for research, Cem. Concr. Res. 112 (2018) 1037–1049, https://doi.org/10.1016/j.cemconres.2018.05.006. https://www.sciencedirect.com/science/article/pii/S0008884617311924.
[3] T. Wangler, N. Roussel, F.P. Bos, T.A.M. Salet, R.J. Flatt, Digital concrete: a review, Cem. Concr. Res. 123 (2019), 105780.
[4] G. De Schutter, K. Lesage, V. Mechtcherine, V.N. Nerella, G. Habert, I. Agusti-Juan, Vision of 3D printing with concrete — technical, economic and environmental potentials, Cem. Concr. Res. 112 (2018) 25–36.
[5] Y.W.D. Tay, B. Panda, S.C. Paul, N.A.N. Mohamed, M.J. Tan, K.F. Leong, 3D printing trends in building and construction industry: a review, Virtual Phys. Prototyp. 12 (2017) 261–276.
[6] J. Buchli, M. Giftthaler, N. Kumar, M. Lussi, T. Sandy, K. Dörfler, N. Hack, Digital in situ fabrication - challenges and opportunities for robotic in situ fabrication in architecture, construction, and beyond, Cem. Concr. Res. 112 (2018) 66–75.
[7] F. Bos C. Menna M. Pradena E. Kreiger W.R. Leal da Silva A.U. Rehman D. Weger R.J.M. Wolfs Y. Zhang L. Ferrara V. Mechtcherine , The realities of additively manufactured concrete structures in practice, Cem. Concr. Res. (accepted).
[8] D. Asprone, C. Menna, F.P. Bos, T.A.M. Salet, J. Mata-Falcón, W. Kaufmann, Rethinking reinforcement for digital fabrication with concrete, Cem. Concr. Res. 112 (2018) 111–121.
[9] C. Menna, J. Mata-Falcón, F.P. Bos, G. Vantyghem, L. Ferrara, D. Asprone, T. Salet, W. Kaufmann, Opportunities and challenges for structural engineering of digitally fabricated concrete, Cem. Concr. Res. 133 (2020), 106079.
[10] apis cor realizes russia's first on-site 3D printed house in just 24 hours. https://www.designboom.com/architecture/apis-cor-pik-3d-printed-house-24-hours-02-28-2017/, 2017 (accessed November 8, 2021).
[11] D. Kamin, How an 11-foot-tall 3-d printer is helping to create a community, The New York Times, 2021. https://www.nytimes.com/2021/09/28/business/3D-printing-homes.html.
[12] A. Bendix, These 3D-printed homes can be built for less than $4,000 in just 24 hours, Business Insider, 2019. https://www.businessinsider.com/3d-homes-that-take-24-hours-and-less-than-4000-to-print-2018-9.
[13] The truth: facts about the true state of the art of 3d construction printing, COBOD International A/S, 2019. https://cobod.com/wp-content/uploads/2019/12/3DCP-fact-sheet-Final.pdf.
[14] B.N. Diggs-McGee, E.L. Kreiger, M.A. Kreiger, M.P. Case, Print time vs. elapsed time: a temporal analysis of a continuous printing operation for additive constructed concrete, Addit. Manuf. 28 (2019) 205–214.
[15] Y. Chen, S. Chaves Figueiredo, Z. Li, Z. Chang, K. Jansen, O. Çopuroğlu, E. Schlangen, Improving printability of limestone-calcined clay-based cementitious materials by using viscosity-modifying admixture, Cem. Concr. Res. 132 (2020), 106040.
[16] F. Boscaro, E. Quadranti, T. Wangler, S. Mantellato, L. Reiter, R.J. Flatt, Eco-friendly, set-on-demand digital concrete, 3D Print. Addit. Manuf. (2021), https://doi.org/10.1089/3dp.2020.0350.
[17] S. Bhattacherjee, A.S. Basavaraj, A.V. Rahul, M. Santhanam, R. Gettu, B. Panda, E. Schlangen, Y. Chen, O. Copuroglu, G. Ma, L. Wang, M.A. Basit Beigh, V. Mechtcherine, Sustainable materials for 3D concrete printing, Cem. Concr. Compos. 122 (2021), 104156.
[18] M. Mohammad, E. Masad, S.G. Al-Ghamdi, 3D concrete printing sustainability: a comparative life cycle assessment of four construction method scenarios, Buildings 10 (2020) 245.
[19] W.R. Leal da Silva M. Kaasgaard , Green concrete for sustainable 3DCP, Concr. Int. (submitted).
[20] E.L. Kreiger, M.A. Kreiger, M.P. Case, Development of the construction processes for reinforced additively constructed concrete, Addit. Manuf. 28 (2019) 39–49.
[21] BOD2 specifications, COBOD International A/S, 2019. https://cobod.com/wp-content/uploads/2020/09/BOD2-Specifications-1.pdf.
[22] J.J. Burger T. Wangler Y.-H. Chiu C. Techathuvanun F. Gramazio M. Kohler E. Lloret Fritschi , Material informed formwork geometry, in: S.V.T. Bojan (Ed.), Towards a New, Configurable Architecture (ECAADe 2021), n.d.: pp. 199–208.
[23] E.L. Paul, Handbook of Industrial Mixing: Science and Practice, Wiley-Interscience, Hoboken, N.J., 2004.
[24] A.W. Nienow, M.F. Edwards, N. Harnby, Mixing in the Process Industries, Second Edition, Butterworth-Heinemann, 1997.
[25] P.J. Cullen, R.J. Romañach, N. Abatzoglou, C.D. Rielly, Pharmaceutical Blending and Mixing, John Wiley & Sons, 2015.
[26] O. Levenspiel, Chemical Reaction Engineering, Wiley, 1999.
[27] V. Mechtcherine, F.P. Bos, A. Perrot, W.R.L. da Silva, V.N. Nerella, S. Fataei, R.J. M. Wolfs, M. Sonebi, N. Roussel, Extrusion-based additive manufacturing with cement-based materials – production steps, processes, and their underlying physics: a review, Cem. Concr. Res. 132 (2020), 106037.
[28] C. Gosselin, R. Duballet, P. Roux, N. Gaudillière, J. Dirrenberger, P. Morel, Large-scale 3D printing of ultra-high performance concrete – a new processing route for architects and builders, Mater. Des. 100 (2016) 102–109.
[29] ACI PRC-304.6-09, Guide for Use of Volumetric-Measuring and Continuous-Mixing Concrete Equipment, 2019. Reapproved.
[30] O. Mazanec, D. Lowke, P. Schießl, Mixing of high performance concrete: effect of concrete composition and mixing intensity on mixing time, Mater. Struct. 43 (2010) 357–365.
[31] C.F. Ferraris, Concrete mixing methods and concrete mixers: state of the art, J. Res. Natl. Inst. Stand. Technol. 106 (2001) 391–399.
[32] B. Cazacliu, N. Roquet, Concrete mixing kinetics by means of power measurement, Cem. Concr. Res. 39 (2009) 182–194.
[33] P. Juilland, A. Kumar, E. Gallucci, R.J. Flatt, K.L. Scrivener, Effect of mixing on the early hydration of alite and OPC systems, Cem. Concr. Res. 42 (2012) 1175–1188.
[34] D. Han, R.D. Ferron, Influence of high mixing intensity on rheology, hydration, and microstructure of fresh state cement paste, Cem. Concr. Res. 84 (2016) 95–106.
[35] J. Dils, G. De Schutter, V. Boel, Influence of mixing procedure and mixer type on fresh and hardened properties of concrete: a review, Mater. Struct. 45 (2012) 1673–1683.
[36] R.J.M. Wolfs, F.P. Bos, T.A.M. Salet, Early age mechanical behaviour of 3D printed concrete: numerical modelling and experimental testing, Cem. Concr. Res. 106 (2018) 103–116.
[37] A.M. Neville, Properties of Concrete, Pearson, 2011.
[38] J. Ravlic, Can you provide information about nozzles and printheads?. https://cobod.com/faq-items/can-you-provide-information-about-nozzles-and-printheads/, 2020.
[39] A. Perrot, A. Pierre, V.N. Nerella, R.J.M. Wolfs, E. Keita, S.A.O. Nair, N. Neithalath, N. Roussel, V. Mechtcherine, From analytical methods to numerical simulations: a process engineering toolbox for 3D concrete printing, Cem. Concr. Compos. 122 (2021), 104164.
[40] V. Mechtcherine, S. Fataei, F.P. Bos, R.A. Buswell, W.R.L. da Silva, E. Keita, H. W. Krauss, D. Lowke, A. Perrot, V.N. Nerella, N. Roussel, M. Sonebi, T. Wangler, D. Weger, R. Wolfs, Digital fabrication with cement-based materials: underlying physics, in: N. Roussel, D. Lowke (Eds.), Digital Fabrication with Cement-Based Materials: State-of-the-Art Report of the RILEM TC 276-DFC, Springer International Publishing, Cham, 2022, pp. 49–98.
[41] G. De Schutter, D. Feys, Pumping of fresh concrete: insights and challenges, RILEM Tech. Lett. 1 (2016) 76–80.
[42] S.H. Kwon, K.P. Jang, J.H. Kim, S.P. Shah, State of the art on prediction of concrete pumping, international journal of concrete, Struct. Mater. 10 (2016) 75–85.
[43] M. Choi, N. Roussel, Y. Kim, J. Kim, Lubrication layer properties during concrete pumping, Cem. Concr. Res. 45 (2013) 69–78.
[44] L. Reiter, T. Wangler, A. Anton, R.J. Flatt, Setting on demand for digital concrete – principles, measurements, chemistry, validation, Cem. Concr. Res. 132 (2020), 106047.

[45] Y. Tao, A.V. Rahul, K. Lesage, Y. Yuan, K. Van Tittelboom, G. De Schutter, Stiffening control of cement-based materials using accelerators in inline mixing processes: possibilities and challenges, Cem. Concr. Compos. 119 (2021), 103972.
[46] E.Lloret Fritschi, L. Reiter, T. Wangler, F. Gramazio, M. Kohler, R.J. Flatt, Smart dynamic casting: slipforming with flexible formwork - inline measurement and control, in: HPC/CIC Tromsø 2017, Norwegian Concrete Association, 2017.
[47] A. Szabo, L. Reiter, E. Lloret-Fritschi, F. Gramazio, M. Kohler, R.J. Flatt, Mastering yield stress evolution and formwork friction for smart dynamic casting, Materials 13 (2020), https://doi.org/10.3390/ma13092084.
[48] V. Esnault, A. Labyad, M. Chantin, F. Toussaint, Experience in online modification of rheology and strength acquisition of 3D printable mortars, in: T. Wangler, R. J. Flatt (Eds.), First RILEM International Conference on Concrete and Digital Fabrication – Digital Concrete 2018, Springer International Publishing, 2019, pp. 24–38.
[49] Y. Tao, A.V. Rahul, K. Lesage, K. Van Tittelboom, Y. Yuan, G. De Schutter, Mechanical and microstructural properties of 3D printable concrete in the context of the twin-pipe pumping strategy, Cem. Concr. Compos. 125 (2022), 104324.
[50] N. Roussel, Rheological requirements for printable concretes, Cem. Concr. Res. 112 (2018) 76–85.
[51] E. Lloret-Fritschi, T. Wangler, L. Gebhard, J. Mata-Falcón, S. Mantellato, F. Scotto, J. Burger, A. Szabo, N. Ruffray, L. Reiter, F. Boscaro, W. Kaufmann, M. Kohler, F. Gramazio, R. Flatt, From smart dynamic casting to a growing family of digital casting systems, Cem. Concr. Res. 134 (2020), 106071.
[52] D. Hwang, B. Khoshnevis, Concrete wall fabrication by contour crafting, in: Proceedings of the 21st International Symposium on Automation and Robotics in Construction, International Association for Automation and Robotics in Construction (IAARC), 2004, https://doi.org/10.22260/isarc2004/0057.
[53] N. Hack, H. Kloft, Shotcrete 3D printing technology for the fabrication of slender fully reinforced freeform concrete elements with high surface quality: a real-scale demonstrator, in: Second RILEM International Conference on Concrete and Digital Fabrication, Springer International Publishing, 2020, pp. 1128–1137.
[54] J.G. Sanjayan, B. Nematollahi, M. Xia, T. Marchment, Effect of surface moisture on inter-layer strength of 3D printed concrete, Constr. Build. Mater. 172 (2018) 468–475.
[55] E. Keita, H. Bessaies-Bey, W. Zuo, P. Belin, N. Roussel, Weak bond strength between successive layers in extrusion-based additive manufacturing: measurement and physical origin, Cem. Concr. Res. 123 (2019), 105787.
[56] H.S. Fogler, Elements of Chemical Reaction Engineering, Prentice Hall, 1999.
[57] J.B. Rawlings, J.G. Ekerdt, Chemical reactor analysis and design fundamentals, Nob Hill Publishing, 2002.
[58] P.V. Danckwerts, Continuous flow systems: distribution of residence times, Chem. Eng. Sci. 2 (1953) 1–13.
[59] T. Wangler, F. Scotto, E. Lloret-Fritschi, R.J. Flatt, Residence time distributions in continuous processing of concrete, in: Rheology and Processing of Construction Materials, 2019, https://doi.org/10.1007/978-3-030-22566-7_52.
[60] E.B. Nauman, Residence time distributions, in: Handbook of Industrial Mixing, John Wiley & Sons, Ltd, 2004, pp. 1–17.
[61] L. Reiter, T. Wangler, N. Roussel, R.J. Flatt, The role of early age structural build-up in digital fabrication with concrete, Cem. Concr. Res. 112 (2018) 86–95.
[62] E.B. Nauman, B.A. Buffham, Mixing in Continuous Flow Systems, John Wiley & Sons Inc, New York, 1983.
[63] R.A. Buswell, W.R.L. da Silva, F.P. Bos, H.R. Schipper, D. Lowke, N. Hack, H. Kloft, V. Mechtcherine, T. Wangler, N. Roussel, A process classification framework for defining and describing digital fabrication with concrete, Cem. Concr. Res. 134 (2020), 106068.
[64] F.E. Golling, R. Pires, A. Hecking, J. Weikard, F. Richter, K. Danielmeier, D. Dijkstra, Polyurethanes for coatings and adhesives – chemistry and applications, Polym. Int. 68 (2019) 848–855.
[65] Technology. https://www.iconbuild.com/technology (accessed November 8, 2021).
[66] T.T. Le, S.A. Austin, S. Lim, R.A. Buswell, A.G.F. Gibb, T. Thorpe, Mix design and fresh properties for high-performance printing concrete, Mater. Struct. 45 (2012) 1221–1232.
[67] S. Lim, R.A. Buswell, T.T. Le, R. Wackrow, S.A. Austin, A.G.F. Gibb, T. Thorpe, Development of a viable concrete printing process, in: Proceedings of the 28th ISARC, Seoul, Korea, 2011, pp. 665–670.
[68] CyBe MORTAR, CyBe construction. https://cybe.eu/technology/cybe-mortar/, 2019 (accessed October 31, 2021).
[69] Y. Weng, M. Li, S. Ruan, T.N. Wong, M.J. Tan, K.L. Ow Yeong, S. Qian, Comparative economic, environmental and productivity assessment of a concrete bathroom unit fabricated through 3D printing and a precast approach, J. Clean. Prod. 261 (2020), 121245.
[70] Sika Group, 3D concrete printing. https://www.sika.com/en/knowledge-hub/3d-concrete-printing.html (accessed November 26, 2021).
[71] Baumit BauMinator , (n.d.). https://en.calameo.com/read/001102318ccb73a8929fc (accessed November 26, 2021).
[72] A. Anton, L. Reiter, T. Wangler, V. Frangez, R.J. Flatt, B. Dillenburger, A 3D concrete printing prefabrication platform for bespoke columns, Autom. Constr. 122 (2021), 103467.
[73] L. Reiter A.-M. Anton T. Wangler R.J. Flatt , Layered Extrusion - Processing and Set on Demand, (n.d.).
[74] V.N. Nerella, S. Hempel, V. Mechtcherine, Effects of layer-Interface properties on mechanical performance of concrete elements produced by extrusion-based 3D-printing, Constr. Build. Mater. 205 (2018) 586–601.
[75] Y.W.D. Tay, G.H.A. Ting, Y. Qian, B. Panda, L. He, M.J. Tan, Time gap effect on bond strength of 3D-printed concrete, Virtual Phys. Prototyp. 14 (2019) 104–113.
[76] C. Kamp, Eerste geprint huis in Europa op Kamp C - First printed house in Europe at Kamp C. https://www.youtube.com/watch?v=pxrVEfxrwUw, 2020 (accessed November 9, 2021).
[77] ICON and TMD unveil 3D-printed barracks to house women & men during military training in Texas, (n.d.). https://www.iconbuild.com/updates/icon-and-tmd-unveil-3d-printed-barracks-to-house-women-and-men (accessed November 9, 2021).
[78] A. Perrot, D. Rangeard, A. Pierre, Structural built-up of cement-based materials used for 3D-printing extrusion techniques, Mater. Struct. 49 (2015) 1213–1220.
[79] T. Wangler, E. Lloret, L. Reiter, N. Hack, F. Gramazio, M. Kohler, M. Bernhard, B. Dillenburger, J. Buchli, N. Roussel, R. Flatt, Digital concrete: opportunities and challenges, RILEM Tech. Lett. 1 (2016) 67–75.
[80] J. Kruger, S. Zeranka, G. van Zijl, 3D concrete printing: a lower bound analytical model for buildability performance quantification, Autom. Constr. 106 (2019), 102904.
[81] A.S.J. Suiker, Mechanical performance of wall structures in 3D printing processes: theory, design tools and experiments, Int. J. Mech. Sci. 137 (2018) 145–170.
[82] A.S.J. Suiker, R.J.M. Wolfs, S.M. Lucas, T.A.M. Salet, Elastic buckling and plastic collapse during 3D concrete printing, Cem. Concr. Res. 135 (2020), 106016.
[83] N. Roussel, G. Ovarlez, S. Garrault, C. Brumaud, The origins of thixotropy of fresh cement pastes, Cem. Concr. Res. 42 (2012) 148–157.
[84] J. Mewis, N.J. Wagner, Thixotropy, Adv. Colloid Interf. Sci. 147–148 (2009) 214–227.
[85] L.E. Burris, K.E. Kurtis, Influence of set retarding admixtures on calcium sulfoaluminate cement hydration and property development, Cem. Concr. Res. 104 (2018) 105–113.
[86] A.S.J. Suiker, Effect of accelerated curing and layer deformations on structural failure during extrusion-based 3D printing, Cem. Concr. Res. 151 (2022), 106586.
[87] R.J.M. Wolfs, F.P. Bos, T.A.M. Salet, Triaxial compression testing on early age concrete for numerical analysis of 3D concrete printing, Cem. Concr. Compos. 104 (2019), 103344.
[88] F.P. Bos, P.J. Kruger, S.S. Lucas, G.P.A.G. van Zijl, Juxtaposing fresh material characterisation methods for buildability assessment of 3D printable cementitious mortars, Cem. Concr. Compos. 120 (2021), 104024.
[89] L. Fullard, C. Davies, Minimising the spread of residence-time distribution for flat and heaped powders in a wedge-shaped planar hopper, Particuology 30 (2017) 102–110.
[90] S. Golshan, B. Esgandari, R. Zarghami, B. Blais, K. Saleh, Experimental and DEM studies of velocity profiles and residence time distribution of non-spherical particles in silos, Powder Technol. 373 (2020) 510–521.
[91] L. Reiter, M. Palacios, T. Wangler, R.J. Flatt, in: Putting Concrete to Sleep and Waking It Up With Chemical Admixtures 302, ACI Special Publication, 2015, pp. 145–154.
[92] XtreeE | The large-scale 3d, (n.d.). https://xtreee.com/ (accessed November 26, 2021).
[93] G.B. Tatterson, Scaleup and Design of Industrial Mixing Processes, McGraw-Hill New York, 1994.
[94] M. Zlokarnik, Stirring: Theory and Practice, Wiley-VCH, 2001.
[95] R.K. Grenville, A.W. Nienow, Blending of miscible liquids, in: Handbook of Industrial Mixing, John Wiley & Sons Inc, Hoboken, NJ, USA, 2004, pp. 507–542.
[96] L.K. Mettler, F.K. Wittel, R.J. Flatt, H.J. Herrmann, Evolution of strength and failure of SCC during early hydration, Cem. Concr. Res. 89 (2016) 288–296.
[97] D. Marchon, S. Kawashima, H. Bessaies-Bey, S. Mantellato, S. Ng, Hydration and rheology control of concrete for digital fabrication: potential admixtures and cement chemistry, Cem. Concr. Res. 112 (2018) 96–110.
[98] R.R. Hemrajani, G.B. Tatterson, Mechanically stirred vessels, in: Handbook of Industrial Mixing, John Wiley & Sons, Inc, Hoboken, NJ, USA, 2004, pp. 345–390.
[99] M.K. Mohan, A.V. Rahul, K. Van Tittelboom, G. De Schutter, Rheological and pumping behaviour of 3D printable cementitious materials with varying aggregate content, Cem. Concr. Res. 139 (2021), 106258.
[100] V. Novák, F. Rieger, Homogenization efficiency of helical ribbon and anchor agitators, Chem. Eng. J. 9 (1975) 63–70.
[101] V. Uhl, Mixing V1: Theory and Practice, Elsevier, 2012.
[102] M.S. de França, B. Cazacliu, F.A. Cardoso, R.G. Pileggi, Influence of mixing process on mortars rheological behavior through rotational rheometry, Constr. Build. Mater. 223 (2019) 81–90.
[103] M.S. Rebmann, R.G. Pileggi, Influence of aggregate particle size distribution on mixing behavior and rheological properties of low-binder concrete, in: Rheology and Processing of Construction Materials, Springer International Publishing, 2020, pp. 43–51.
[104] J.H. Marden, L.R. Allen, Molecules, muscles, and machines: universal performance characteristics of motors, Proc. Natl. Acad. Sci. U. S. A. 99 (2002) 4161–4166.
[105] K. Dermitzakis, J.P. Carbajal, J.H. Marden, Scaling Laws in robotics, Procedia Comput. Sci. 7 (2011) 250–252.
[106] E. Brito-De La Fuente, L. Choplin, P.A. Tanguy, Mixing with helical ribbon impellers: effect of highly shear thinning behaviour and impeller geometry, Chem. Eng. Res. Des. 75 (1997) 45–52.
[107] D.S. Dickey, J.B. Fasano, Mechanical design of mixing equipment, in: Handbook of Industrial Mixing, John Wiley & Sons Inc, Hoboken, NJ, USA, 2004, pp. 1247–1332.
[108] K. Suzumori, A.A. Faudzi, Trends in hydraulic actuators and components in legged and tough robots: a review, Adv. Robot. 32 (2018) 458–476.
[109] Materials – 3D Concrete Printing Weber, (n.d.). https://www.3d.weber/materials/ (accessed February 11, 2022).

[110] N. Roussel (Ed.), Understanding the Rheology of Concrete, Woodhead Publishing, 2012.
[111] A.B. Metzner, R.E. Otto, Agitation of non-newtonian fluids, AIChE J. 3 (1957) 3–10.
[112] D. Doraiswamy, R.K. Grenville, A.W. Etchells, Two-score years of the Metzner-Otto correlation, Ind. Eng. Chem. Res. 33 (1994) 2253–2258.
[113] G. Delaplace, R. Jeantet, R. Grenville, G. Cuvelier, K. Loubiere, How dimensional analysis allows to go beyond metzner-Otto concept for non-newtonian fluids, Rev. Chem. Eng. (2020), https://doi.org/10.1515/revce-2020-0006.
[114] V. Mechtcherine, V.N. Nerella, F. Will, M. Näther, J. Otto, M. Krause, Large-scale digital concrete construction – CONPrint3D concept for on-site, monolithic 3D-printing, Autom. Constr. 107 (2019), 102933.
[115] F. Bos, Z. Ahmed, E. Jutinov, T. Salet, F.P. Bos, Z.Y. Ahmed, E.R. Jutinov, T.A. M. Salet, Experimental exploration of metal cable as reinforcement in 3D printed concrete, Materials 10 (2017) 1314.
[116] N. Zhang, M. Xia, J. Sanjayan, Short-duration near-nozzle mixing for 3D concrete printing, Cem. Concr. Res. 151 (2022), 106616.